MCP Papers in Press. Published on March 18, 2014 as Manuscript M113.034322

Structural and Functional Analysis of Novel Human Cytochrome *c* Targets in Apoptosis

Running Title: Novel Human Cytochrome *c* Targets

Jonathan Martínez-Fábregas[1], Irene Díaz-Moreno[1], Katiuska González-Arzola[1], Simon Janocha[2], José A. Navarro[1], Manuel Hervás[1], Rita Bernhardt[2], Adrian Velazquez-Campoy[3], Antonio Díaz-Quintana[1], Miguel Á. De la Rosa[1,*]

[1] Instituto de Bioquímica Vegetal y Fotosíntesis, cicCartuja, Universidad de Sevilla-CSIC, Avda. Américo Vespucio 49, Sevilla 41092, Spain.

[2] Institut für Biochemie, Universität des Saarlandes, Campus B2.2, D-66123 Saarbrücken, Germany

[3] Instituto de Biocomputación y Física de Sistemas complejos (BIFI), Universidad de Zaragoza, C/ Mariano Esquillor, Zaragoza 50018, Spain.

Contact:

Correspondence should be addressed to: Miguel A. De la Rosa

Email: marosa@us.es

Phone Number: +34 954489510

Fax Number: +34 954460065

ABBREVIATIONS

Apaf-1 – Apoptosis protease-activating factor-1

BiFC – Bimolecular fluorescence complementation

C*c* – Cytochrome *c*

CED-4 – Cell-death abnormality-4

CPT – Camptothecin

CSP – Chemical shift perturbation

DAPI – 4', 6-diamidino-2-phenylindole

Dark – Drosophila Apaf-1-related killer

DMEM – Dulbecco's modified Eagle's medium

EGFP – Enhanced green fluorescent protein

ITC – Isothermal titration calorimetry

NMR – Nuclear magnetic resonance

PCD – Programmed cell death

SPR – Surface plasmon resonance

TS-4B – Thiol-Sepharose 4B

YFP – Yellow fluorescent protein

SUMMARY

Since the first description of apoptosis four decades ago, great efforts have been made to elucidate, both *in vivo* and *in vitro*, the molecular mechanisms involved in its regulation. Although the role of cytochrome *c* during apoptosis is well-established, relatively little is known about its participation in signaling pathways *in vivo* due to its essential role during respiration. To better understand the role of cytochrome *c* in the onset of apoptosis, a proteomic approach based on affinity chromatography with cytochrome *c* as bait was used in this study. In this approach, novel cytochrome *c* interaction partners were identified whose *in vivo* interaction, as well as cellular localization, were facilitated through bimolecular fluorescence complementation. Modeling of the complexes interface between cytochrome *c* and its counterparts indicated the involvement of the surface surrounding the heme crevice of cytochrome *c*, in agreement with the vast majority of known redox adducts of cytochrome *c*. However, in contrast to the high turnover rate of the mitochondrial cytochrome *c* redox adducts, those occurring under apoptosis lead to the formation of stable nucleo-cytoplasmic ensembles, as inferred mainly from surface plasmon resonance and nuclear magnetic resonance measurements, which have permitted us to corroborate the formation of such complexes *in vitro*. The results obtained suggest that human cytochrome *c* interacts with pro-survival, anti-apoptotic proteins following its release into the cytoplasm. Thus, cytochrome *c* may interfere with cell survival pathways and unlock apoptosis in order to prevent the spatial and temporal co-existence of antagonist signals.

INTRODUCTION

Apoptosis, an event that is both morphologically distinguishable from other types of cell death (e.g., senescence or necrosis) and tightly regulated from a genetic and biochemical point of view, controls tissue homeostasis and eliminates damaged cells in mammals [1]. The process is characterized by the co-occurrence of nuclear and cytoplasmic condensation, blebbing of cytoplasmic membranes and the emergence of apoptotic bodies as a consequence of cell fragmentation [2].

The main processes characterizing apoptosis are driven by a cascade of proteolytic events mediated by caspases (cysteine-dependent aspartate-specific proteases), a subfamily of cysteine proteases [3]. Two different pathways – extrinsic, or death receptor-initiated [4], and intrinsic, or mitochondrial [5], pathways – are involved in the activation of these proteolytic events. DNA damage, oxidative stress and growth factor deprivation are well-known apoptosis inducers that activate the intrinsic pathway [6], involving the permeabilization of the outer mitochondrial membrane. This event occurs prior to the release of pro-apoptotic factors (e.g., AIF, cytochrome *c* [C*c*], Smac/DIABLO and HtrA2/Omi) from the mitochondrial intermembrane space into the cytoplasm.

C*c* is a well-known heme protein which plays an essential role in homeostasis and apoptosis. With regard to the former, C*c* acts as an electron shuttle between complexes III and IV in mitochondrial respiration. In apoptosis, on the other hand, C*c* is released from mitochondria into the cytoplasm. During this process, cytosolic C*c* and dATP bind to apoptosis protease-activating factor-1 (Apaf-1), forming the apoptosome – a macromolecular platform –, which, in turn, leads to the activation of initiator caspases [7,8].

Under homeostatic conditions, C*c* is kept in the mitochondrial space, where its concentration can reach 0.5-5 mM [9]. Notably, approximately 90 % of mitochondrial C*c* content is sequestered within the cristae of the inner membrane and, therefore, is unavailable for electron transport [10]. Moreover, the interaction of C*c* with Apaf-1, leading to apoptosome formation, is one of the

earliest events to occur at the onset of apoptosis, a process requiring small amounts of the heme protein due to the amplification of its effect by the proteolytic cascade. C*c* concentration in the intermembrane space is, therefore,extremely high, leading one to wonder whether C*c* is also regulating other processes during programmed cell death (PCD).

Beyond the well-established *in vitro* role of C*c* during apoptosis in mammals, newly-proposed putative functions of the heme protein in cell death signaling remain controversial. Some authors suggest that C*c* exclusively induces apoptosome formation and caspase activation in the cytosol [11]. Others have recently proposed the existence of additional, not yet fully understood C*c* functions in the pro-apoptotic response, both in the nucleus [12,13] and the endoplasmic reticulum [14,15,16].

Even though a function for cytosolic C*c* during PCD has been defined only in mammals [8], the mitochondria-to-cytoplasm release of C*c* is an evolutionarily conserved event found in yeast [17], plants [18], flies [19] and mammals [20].

The specific role of C*c* in apoptosis signaling has not been extensivelyinvestigated *in vivo* due to the difficulty of obtaining C*c* knockout mutants. Recently, Vempati *et al*. [21] were able to produce a C*c* knockout mutant in mice fibroblasts. Intriguingly, this mutant was resistant to pro-apoptotic agents acting through both the intrinsic and extrinsic pathways. Meriting particular interest, apoptosis can normally be activated in mutants lacking Apaf-1, the only apoptotic partner of C*c* described *in vivo* thus far [22,23].

The different phenotypes of C*c* and Apaf-1 knockouts and the high concentration of C*c* in the mitochondrial intermembrane space cannot be explained if C*c* is restrained from interacting with Apaf-1 during PCD. However, these can be easily harmonized if a broader, critical role for C*c* in the regulation of life and death decisions is considered, as recently proposed by Hüttemann *et al*. [24].

To facilitate the identification of putative novel C*c* interaction partners here, a proteomic approach was developed based on affinity chromatography coupled with MALDI-TOF/TOF. The use of bimolecular fluorescence complementation (BiFC) permitted the corroboration of not only the *in vivo* interaction, but also to determine the *in cell* localization of such novel C*c* complexes. Moreover, C*c* complexes involving ALDOA, ANP32B, eIF2α, SET, STRAP and YWHAE were modeled *in silico* using docking algorithms. *In vitro* validation through surface plasmon resonance (SPR) was performed only for C*c* complexes including protein interaction partners expressed in a soluble form, that is, eIF2α, hnRNP C1/C2, HSPA5, SET and YWHAE. Furthermore, nuclear magnetic resonance (NMR) and isothermal titration calorimetry (ITC) measurements were performed to delve into the complex formation. The qualitative methodological approach herein proposed combines proteomic tools with other complementary techniques, namely BiFC, SPR, NMR and ITC to further corroborate the reliability of the novel C*c*-involving protein interactions and to characterize the nature of such complexes from both the structural and functional point of view. Two major advantages should be highlighted. First, the synergy between all these techniques reduces the rate of false positives and avoids the need for proteomic replicas; and second, the BiFC experiments, combined with SPR, NMR and ITC approaches, provide extra information not only on the cellular compartment at which the protein-protein interactions take place but also on the specificity and lifetime of the C*c*-involving complexes.

In addition to the assembly of the apoptotic platform during apoptosis, the results obtained in this study might suggest that C*c* is also involved in other signaling pathways, interfering with cell survival and unlocking apoptosis. Indeed, C*c* appears to abolish the co-existence of pro-survival and pro-apoptotic signals. The additional functions, besides apoptosome assembly, ascribed to C*c* during apoptosis therefore suggest an evolutionarily conserved role for C*c* during PCD and may explain its release from mitochondria in the majority of organisms.

EXPERIMENTAL PROCEDURES

Expression and Purification of C*c* E104C Mutant

Plasmid *p*Cyt*H* [25], containing the coding region of human C*c*, was used as a template to obtain the E104C C*c* mutant, in which the glutamate at the C-terminal end was replaced by a cysteine, through site-directed mutagenesis. The oligonucleotides employed to build the E104C species were 5'-gcgaccaattgctgatgaattc-3' and 3'-cgctggttaacgactacttaag-5'. The E104C C*c* was expressed and further purified using ionic exchange chromatography, a process previously described by Rodríguez-Roldán *et al.* [25].

Jurkat T-Cell Cultures and Apoptosis Induction

Jurkat human T-lymphoma cells were cultured in RPMI 1640 (PAA) supplemented with 10 % heat-inactivated fetal bovine serum (PAA), 2 mM L-glutamine (Gibco), 100 $U \cdot mL^{-1}$ streptomycin (Gibco) and 100 $\mu g \cdot mL^{-1}$ penicillin (Gibco) at 37 °C in a humidified atmosphere of 5% CO_2 / 95% air. Cells were grown as exponentially growing confluent monolayer in 645 mL flasks (Nunc) with the medium refreshed every 48 h.

Apoptosis was induced in Jurkat human T-lymphoma cells with 10 μM camptothecin (CPT; Calbiochem) for up to 6 h [26] in order to ensure the release of C*c* from mitochondria into the cytosol [27].

DAPI Staining

Non-treated or treated Jurkat T cells with 10 μM of CPT were harvested by centrifugation at 1,000 x g for 5 min, resuspended in PBS containing 500 $ng \cdot mL^{-1}$ DAPI and incubated for 30 min at room temperature. Cells on glass slides were examined under a fluorescence microscope equipped with a DAPI filter and apoptotic cells were identified by the presence of densely stained granular nuclear apoptotic bodies.

Flow Cytometry Measurements

Jurkat T cells, non-treated or treated with 10 μM of CPT, were harvested as described above, and fixed in ethanol 70 % for 1 h. Cells were resuspended in a propidium iodide (PI) solution as previously described [28], to be further incubated for 1 h at 37 °C and analyzed by flow cytometry using a Becton-Dickinson FACS Vantage flow cytometer. Cells with sub-G1 DNA content were considered to be apoptotic.

DNA Fragmentation Assay

Apoptosis was induced in Jurkat T cells with 10 μM CPT for 0, 6, 10 and 24 h and DNA fragmentation assay was carried out as previously described [29]. Briefly, cells were harvested by centrifugation at 1,000 x g for 5 min, washed twice in PBS, resuspended and incubated at 37 °C overnight with 500 μL of buffer D (100 mM Tris-HCl [pH 8.5], 5 mM EDTA, 0.2 M NaCl, 0.2 % [w/v] SDS and 0.2 $mg \cdot mL^{-1}$ proteinase K). Then, 1.5 M NaCl was added and cellular debris was removed by centrifugation at 12,000 x g for 15 min. The DNA present in the supernatant was precipitated with an equal volume of 100 % (v/v) ethanol centrifuging at 12,000 x g for 10 min, washed with 70 % ethanol and incubated for 2 h at 37 °C in buffer E (10 mM Tris-HCl [pH 7.5], 1 mM EDTA and 100 $\mu g \cdot mL^{-1}$ DNase-free RNase A). Then, DNA was loaded onto a 2 % agarose gel and electrophoresis was carried out at 50 V for 2 h in 0.5 x TBE buffer.

Cellular Viability Assay

Cell viability was measured using the trypan blue exclusion assay. Jurkat T cells treated with 10 μM CPT for different times (0, 3, 6, 10 and 24 hours) were collected by centrifugation at 1,000 x g for 5 min. Cells were resuspended in trypan blue solution and counted with a hemocytometer. The viability percentage of Jurkat T cells was obtained by dividing the number of viable cells by the total number of cells.

Cell Extract Preparation

Cell extracts from 1.8 L of culture with either untreated or 10 μM CPT-treated Jurkat T cells were prepared for affinity chromatography purification. In both cases, cells were harvested by centrifugation at 1000 x g for 5 min, washed twice in PBS, pelleted again and resuspended to be further lysed by sonication in buffer I (50 mM Tris-HCl [pH 7.5], 50 mM NaCl, 0.25% Triton X-100) supplemented with 1 mM phenylmethylsulfonyl fluoride, 10 $\mu g \cdot mL^{-1}$ aprotinin, 10 $\mu g \cdot mL^{-1}$ leupeptin and 10 $\mu g \cdot mL^{-1}$ of soybean trypsin inhibitor. Cellular debris was then removed through centrifugation at 20,000 x g for 30 min at 4 °C. Protein aliquots were lyophilized and stored at -80 °C.

Purification by Affinity Chromatography

As previously described in Azzi *et al*. [30], affinity chromatography was carried out on a column prepared by the covalent linkage of the C*c* mutant E104C to the Thiol-Sepharose 4B (TS-4B) matrix (Pharmacia). For this preparation, 30 mg of C*c* E104C in 50 mM Tris-HCl (pH 7.5), previously treated with 1 mM DTT to prevent the formation of intermolecular disulfide bridges, was added to a suspension of 4 mL of TS-4B (1 g) resuspended in the same buffer. The suspension, following stirring at 4 °C overnight, was then poured into a Poly-Prep Chromatography Column (Bio-Rad) and washed with 5 mL of 1.5 mM 2-mercaptoethanol / 50 mM Na-acetate (pH 4.5) in order to block unreacted thiol groups. To remove non-covalently bound C*c* E104C, the matrix was washed extensively with 30 mL of 50 mM Tris-HCl (pH 7.5), 1 M NaCl and 1 % Triton X-100. Finally, the column was equilibrated in 50 mM Tris-HCl (pH 7.5). As a control, a TS-4B matrix devoid of C*c* (Blank TS-4B) was prepared following the steps above.

Jurkat T cell extracts, both those untreated and treated with 10 μM of CPT, were loaded into the columns, both with and without C*c*. The columns were then washed with 30 mL of buffer I and 30 mL of buffer II (50 mM Tris-HCl [pH 7.5], 75 mM NaCl) to remove proteins nonspecifically bound. Proteins interacting with greater strength were then eluted with 30 mL of buffer III (50 mM Tris-HCl [pH 7.5], 300 mM NaCl), collected, lyophilized and stored at -80 °C before being analyzed using 2D SDS-PAGE.

Four sets of samples were thus obtained: (1) untreated cell extracts loaded into the Blank TS-4B column, (2) untreated cell extracts loaded into the C*c* TS-4B column, (3) apoptotic cell extracts treated with CPT and purified using the Blank TS-4B column and (4) apoptotic cell extracts treated with CPT and loaded into the C*c* TS-4B column.

2D SDS-PAGE

The protein samples purified as described above were then analyzed using 2D SDS-PAGE. Isoelectrofocusing (IEF) was carried out with the PROTEAN IEF Cell (Bio-Rad) system using 7 cm ReadyStrip IPG Strips (Bio-Rad) with linear pH gradients (pH 3-10). Lyophilized proteins (150 µg) were resuspended in 125 µL rehydration buffer (7 M urea, 2 M thiourea, 2 % CHAPS, 30 mM DTT, 0.5 % Bio-Lyte 3/10 ampholyte and traces of Bromophenol Blue [Bio-Rad]). The ReadyStrip IPG Strips were rehydrated along with the solution containing the protein mixture for 14 h at room temperature.

Samples were later separated in the ReadyStrip IPG Strips for 16000 Vh. IEF gels were then incubated with two equilibration buffers – I (6 M urea, 0.375 M Tris-HCl [pH 8.8], 2 % SDS, 20 % glycerol, 2 % [w/v] DTT) and II (6 M urea, 0.375 M Tris-HCl [pH 8.8], 2 % SDS, 20 % glycerol, 2,5 % [w/v] iodoacetamide) – for 15 min. Finally, the IEF gels were loaded onto a 12 % polyacrylamide gel (8 cm x 7 cm) which was run at 100 V for 2 h in a Mini-PROTEAN 3 Dodeca Cell (Bio-Rad). The 2D gels were stained using Blue Silver [31] and analyzed using the PDQuest 2D Analysis Software Version 8.0.1 (Bio-Rad).

Protein Preparation for Mass Spectrometry

Gel protein spots of interest were manually excised from micro-preparative gels using pipette tips. The selected proteins were reduced in-gel, alkylated and digested with trypsin as described by Sechi and Chait [32]. Briefly, spots were washed twice with water, shrunk for 15 min with 100 % acetonitrile and dried in a Savant SpeedVac for 30 min. Then, the samples were then reduced with 10 mM DTT in 25 mM ammonium bicarbonate for 30 min at 56 ºC and subsequently alkylated with 55 mM iodoacetamide in 25 mM ammonium

bicarbonate for 15 min in the dark. Finally, samples were digested with 12.5 $ng \cdot \mu L^{-1}$ sequencing grade trypsin (Roche Molecular Biochemicals) in 25 mM ammonium bicarbonate (pH 8.5) at 37 ºC overnight.

After digestion, the supernatant was collected from which 1 µL was spotted onto a MALDI target plate and later air-dried at room temperature. Subsequently, 0.4 µL of a 3 $mg \cdot mL^{-1}$ of α-cyano-4-hydroxy-transcinnamic acid matrix (Sigma) in 50 % acetonitrile was added to the dried peptide digest spots and then air-dried at room temperature.

Matrix-Assisted Laser Desorption/Ionization Time-of-Flight Mass Spectrometry (MALDI-TOF MS)

MALDI-TOF MS analyses were performed in a 4800 Proteomics Analyzer MALDI-TOF/TOF mass spectrometer (Applied Biosystems, Framingham, MA) at the Genomics and Proteomics Center, Complutense University of Madrid. Operated in positive reflector mode, with an accelerating voltage of 20000 V. All mass spectra were calibrated internally using peptides from the auto digestion of trypsin.

The analysis by MALDI-TOF/TOF mass spectrometry yields peptide mass fingerprints, and the peptides observed with a S/N ratio greater than 10 can be collated and represented as a list of monoisotopic molecular weights. Proteins ambiguously identified by peptide mass fingerprinting were subjected to MS/MS sequencing analyses using the 4800 Proteomics Analyzer (Applied Biosystems, Framingham, MA). So, from the MS spectra suitable precursors were selected for MS/MS analyses with CID on (atmospheric gas was used) 1 Kv ion reflector mode and precursor mass Windows +/- 5 Da. The plate model and default calibration were optimized for the MS/MS spectra processing.

For protein identification, the UniProtKB-SwissProt_160909 database v. 57.7 (497293 sequences, 175274722 residues) restricted to human protein was searched using a local license of MASCOT 2.1 through the Global Protein Server v 3.6 from Applied Biosystems. Search parameters were:

- Carbamidomethyl Cystein as fixed modification and oxidized methionine as variable modification
- Peptide mass tolerance 50 (PMF) -100 ppm (MSMS or Combined search)
- Peptide charge state +1
- 1 missed trypsin cleavage site
- MS-MS fragments tolerance 0.3 Da

The parameters for the combined search (Peptide mass fingerprint and MS-MS spectra) were the same as above.

In all protein identification, the probability scores were greater than the score fixed by mascot as significant with a p-value lower than 0.05.

Bioinformatics

For protein identification, the UniProtKB-SwissProt database v.57.7 restricted to human protein (20333 sequences) or NCBI database (10084244 sequences) were searched using a local license for MASCOT 2.1. Database search parameters used were the following: trypsin as enzyme; peptide tolerance, 50 ppm for MS analyses and 80 ppm for MS/MS analyses; fragment ion tolerance, 0.3 Da; missed cleavage sites, 1; fixed modification, carbamidomethyl cysteine and variable modifications, methionine oxidation. In all protein identification, probability scores were greater than the score established by MASCOT as significant, with a *p*-value less than 0.05.

Design of Vectors for BiFC Assays

cDNAs coding for C*c* and the proteins identified as C*c* potential targets were purchased (GeneService). The cDNAs were amplified and restriction sites required in each case for further cloning introduced by PCR with the oligonucleotides detailed in the Supplemental Data (see Figure S4 and Table S1). Whereas C*c* cDNA was cloned into the cYFP vector, the cDNAs of the C*c* targets were cloned into the nYFP vector.

As discussed by Hu *et al.* [33], pBiFC-bJunYN155 and pBiFC-bFosYC155 were employed as positive controls, while pBiFC-bJunYN155 and pBiFC-bFosΔZipYC155 were used as negative controls.

BiFC Assays: Human Cell Cultures, Cellular Transfection and Fluorescence Microscopy

HEK293T cells were grown in Dulbecco's modified Eagle's medium (DMEM; PAA) supplemented with 2 mM L-glutamine (Gibco), 100 $U \cdot mL^{-1}$ streptomycin (Gibco), 100 $\mu g \cdot mL^{-1}$ penicillin (Gibco) and 10 % heat-inactivated fetal bovine serum (PAA) at 37 °C in a humidified atmosphere of 5% CO_2 / 95% air. When used for fluorescence microscopy, the HEK293T cells were grown to 80 % confluence in 24-well plates with 500 µL of DMEM, containing 20 mm coverslips. Cells were transiently transfected with the BiFC vectors using the Lipofectamine 2000 Transfection Reagent (Invitrogen) following the manufacturer's instructions. In this way, 0.5 µg of DNA per construct was diluted in 50 µL of Opti-MEM medium (Invitrogen), 2 µL of Lipofectamine was diluted in 50 µL of Opti-MEM medium and the solutions were incubated separately. Following 5 min of incubation at room temperature, both solutions were mixed and incubated for 20 min at room temperature. Finally, 100 µL of the DNA-Lipofectamine mixtures were added to the cells. To favor the protein expression of both constructs, the cells were incubated for 24 h at 37 °C.

Untreated and CPT-treated HEK293T cells on coverslips were mounted in PBS, supplemented with 75 % glycerol and observed under a Leica DM6000 B fluorescence microscope.

Western Blot Analysis

The HEK293T cells transfected with different cDNA vectors were harvested 48 h after transfection through centrifugation at 1,500 rpm for 5 min. Total cell extracts were obtained through repeated freeze-thaw cycles. SDS-PAGE was performed using 12 % polyacrylamide gels. Proteins were transferred onto nitrocellulose membranes (Bio-Rad) using a Mini Trans-Blot (Bio-Rad) and immunoblotted with a rabbit anti-EGFP polyclonal antibody (1:1000; Biovision

Research Products). A horseradish-peroxidase (HRP)-conjugated goat anti-rabbit IgG (1:12000, Sigma-Aldrich) was then used for detection. The immunoreactive bands were developed using ECL Plus Western Blotting Detection System (Amersham).

Docking Protocol

A soft docking algorithm implemented in the Biomolecular Complex Generation with Global Evaluation and Ranking (BiGGER) software package [34] was used to determine *in silico* a model of the complexes between C*c* and some novel interaction partners named earlier. For each run, 5000 solutions were generated using a 15º angular step soft dock and a distance of 7 Å. The center of mass for 50 structures with the best global scores was represented. All graphical images of complexes were generated using the UCSF Chimera package.

Cloning, Expression and Purification of Human Proteins for SPR, ITC and NMR Measurements

Wild-type human C*c* cloned in the pBTR vector under *lac* promoter was expressed in the *E. coli* BL-21(DE3) strain [35]. For this, 25 mL of pre-cultures were grown overnight at 37 ºC in LB medium supplemented with 100 $\mu g \cdot mL^{-1}$ ampicillin. 2.5 mL of pre-culture was used to inoculate 2.5 L of the same medium in a 5 L Erlenmeyer flask. The culture was shaken at 30 ºC for 24 h, after which the cells were harvested at 6,000 rpm for 10 min using a Beckman Coulter Avanti J-25 refrigerated centrifuge. Cells were then resuspended in 1.5 mM borate buffer (pH 8.5), sonicated for 4 min and then centrifuged at 20,000 rpm for 20 min. For NMR measurements, ^{15}N-labeled C*c* was produced in minimal media with $^{15}NH_4Cl$ as nitrogen source. Further purification of wild-type human C*c* was carried out as indicated in Rodríguez-Roldán *et al*. [25].

Proteins interacting with human C*c* – ANP32B, eIF2α, hnRNP C1/C2, HSPA5, SET and YWHAE – were cloned into the pET-28a vector under the T7 promoter using the *Nde*I-*Not*I restriction sites. DNA for cloning was obtained by a PCR reaction using the target cDNA sequences which had been purchased previously (GeneService). DNA inserts coding for C*c* targets were ligated into

the pET-28a vector. Protein expressions were performed in the *E. coli* BL-21 (DE3) RIL strain. 250 mL pre-cultures in LB medium supplemented with 50 $\mu g \cdot mL^{-1}$ kanamycin were grown overnight and then used to inoculate 2.5 L cultures in 5 L flasks. Following the induction of cultures (1 mM IPTG) and growth at 30 ºC for 24 h, cells were harvested at 6,000 rpm for 10 min and resuspended in 40 mL of lysis buffer (20 mM Tris-HCl buffer [pH 8], 0.8 M NaCl, 10 mM imidazole, 0.01 % phenylmethylsulphonyl fluoride [PMSF], 0.2 $mg \cdot mL^{-1}$ lysozyme, 5 mM DTT and 0.02 $mg \cdot mL^{-1}$ DNase), sonicated for 4 min and then centrifuged at 20,000 rpm for 20 min. C*c* counterparts were purified by affinity chromatography. The above lysate was loaded into an Ni-column (Ni Sepharose 6 Fast Flow; GE Healthcare) previously equilibrated with the above buffer and proteins were eluted by the application of an imidazole gradient from 0 to 300 mM. Purity of C*c* targets was checked by running SDS-PAGE. The fractions containing protein were pooled, concentrated by Amicon (10 kDa cut-off membrane) until the protein concentration of 100 µM was reached and dialyzed against 10 mM HEPES buffer (pH 7.4) for SPR measurements, or 5 mM sodium phosphate buffer (pH 6.5) for NMR experiments, or 10 mM sodium phosphate buffer (pH 7.4) for ITC measurements; in all cases, the buffer contained 0.01 % PMSF.

SPR Measurements

The formation of complexes between human C*c* and its protein interaction partners was assayed with SPR using the BiaCore 3000 and CM4 Sensor Chips. An automated desorption procedure was performed prior to each experiment to ensure the cleanliness of the BiaCore tubing, channels and sample injection port. The initial electrostatic attraction of C*c* to the CM4 Sensor Chip surface was assessed by taking into account its isoelectric point and was optimized to pH 5.8. C*c* was then covalently attached to the matrix using standard amine-coupling chemistry, as previously described [36]. A reference flow cell was used as a control in which the chip surface was treated as described above, but without the injection of C*c*.

The binding measurements were performed at 25 ºC using HBS-EP buffer containing 10 mM HEPES, 150 mM NaCl, 3 mM EDTA and 0.005 % surfactant P20 adjusted to pH 7.4. Interactions between C*c* and its protein partners were analyzed by passing several concentrations of C*c*-protein interaction partners (from 0.1 to 10 μM) over the C*c*-modified surface at a flow rate of 10 $\mu L \cdot min^{-1}$. Each concentration was injected at least three times. In each sensorgram, the signals from the reference flow cell surface were subtracted. Between injection cycles, bound proteins were removed following the injection of 10 μL of 10 mM NaOH. In each case, after regeneration the SPR signal reached baseline by flushing with buffer.

NMR Measurements

All protein samples were concentrated in 5 mM sodium phosphate buffer (pH 6.5) using Millipore 3K NMWL centricons and microcons. C*c*-protein partner stock samples ranged in concentration from 200 to 800 μM, and were diluted at a final concentration of 50 μM each in the Shigemi tubes. C*c* was likewise at 50 μM final concentration and reduced upon addition of an aliquot of 0.1 M sodium ascorbate solution up to 4 mM. All NMR samples contained 10% D_2O to adjust the lock signal.

NMR experiments were performed in a Bruker Avance 700 MHz spectrometer at 25 ºC. The interaction of C*c* with its protein partners was followed by acquiring two-dimensional ^{1}H-^{15}N HSQC spectra during titration of 50 μM ^{15}N-C*c* solutions with an increasing amount of each protein partner up to reach a final C*c*:partner molar ratio of 1:1. The pH value of the samples was verified after each titration step. All data processing was performed with Bruker TopSpin 2.0. NMR analyses of chemical-shift perturbations (CSP) were performed with the SPARKY program.

ITC Measurements

All ITC experiments were performed using an Auto-ITC200 instrument (Microcal, GE Healthcare) at 25 ºC by titrating each C*c* protein target with C*c*. The reference cell was filled with distilled water. The experiments consisted of

10 µL injections of 300 µM C*c* in 10 mM sodium phosphate buffer (pH 7.4) into the sample cell, which initially contained 20 µM C*c* protein partner solutions in the same buffer. All the solutions were degassed before the titrations were performed. Titrant was injected at appropriate time intervals to ensure the thermal power signal returned to the baseline prior to the next injection. To achieve homogeneous mixing in the cell, the stirring speed was kept constant at 1000 rpm. The data, specifically the heat per injection normalized per mole of injectant vs. molar ratio, were analyzed with Origin 7 (Microcal). Calibration and performance tests of the calorimeter were carried out conducting $CaCl_2$–EDTA titrations with solutions provided by the manufacturer.

RESULTS

Exploring Novel C*c* Protein Interaction Partners Using a Proteomic Approach

As explained earlier, the identification of novel C*c* protein interaction partners could provide an important starting point for the elucidation of yet unexplored C*c* functions during PCD. Thus, to achieve this goal, a proteomic approach combining affinity chromatography with mass spectrometry was used. A C-end cysteine-substituted C*c* (E104C) was covalently bound to a thiol-sepharose 4B (TS-4B) column using a disulfide bridge. The other two C*c* cysteines did not interfere, as they bind the heme group [37]. A TS-4B column devoid of C*c* (Blank TS-4B) was used as a control.

Jurkat T cell cultures grown in RPMI 1640 medium until reaching a final cell density of 0.15-1.5x10^6 cells·mL^{-1} were used to obtain homeostatic and apoptotic cell extracts. As previously indicated by Johnson *et al.* [26], 10 µM of CPT was used to induce apoptosis in the cultures. To ensure that the cultures were undergoing apoptosis, several characteristic hallmarks were tested. Figure S1.A shows the DNA 'ladder'-shaped fragmentation following 10 h of CPT treatment [29]. This fragmentation is in accord with a positive 4',6-diamidino-2-phenylindole (DAPI) signal fluorescence for nuclei (Figure S1.B) and a lower

DNA content in apoptotic cells followed by flow cytometry (Figure S2). In fact, the population suffering apoptosis upon the addition of CPT was monitored by both flow cytometry and trypan blue dye exclusion (Figure S1.C). Both analyses indicate that the population of cells undergoing apoptosis increased substantially after 6 h of treatment with CPT. Moreover, they show that CPT-treated Jurkat T cells were dying specifically as a result of apoptosis, rather than another type of PCD like necrosis.

Cells were collected for preparation of extracts 6 h following apoptosis induction, the period when C*c* is known to be released from mitochondria into the cytoplasm [38]. Since approximately only 30 % of apoptotic cells were detected by flow cytometry and trypan blue dye exclusion (Figures S1.C and S2), the data collected can be said to address only the early steps of apoptotic signaling. The extracts from both untreated and CPT-treated Jurkat T cells were loaded into the columns both with and without C*c* attached (Figure 1, Left Panel). The putative C*c* protein interaction partners were eluted from the C*c* TS-4B column by increasing ionic strength, whereas the proteins flowing from the Blank TS-4B column served as a control for non-specific binding. The resulting protein fractions were prepared for 2D SDS-PAGE (Figure 1, Left Panel).

From affinity chromatography, four different protein samples were obtained reflecting different experimental conditions: proteins from (a) untreated and (b) CPT-treated cells purified using the blank TS-4B column, as well as proteins from (c) untreated and (d) CPT-treated cells purified with the E104C TS-4B column. The mixture of proteins present in each sample was resolved using 2D SDS-PAGE (Figure S3). PDQuest 2D Analysis Software version 8.0.1 (Bio-Rad) was then used to analyze the resulting 2D gels and the spots highlighted in the master gel image (Figure 1, Right Panel) were identified by MALDI-TOF/TOF and a database search. Table S2 comprehensively summarizes the putative novel C*c*-interacting proteins, along with their cellular localization, identified only in CPT-treated cell extracts or in both untreated and CPT-treated extracts. Using this approach, a list of 21 novel putative C*c* interaction partners have been identified in homeostatic and/or apoptotic Jurkat T cells that it is very likely to contain many false positives (Supplemental Data 1).

In vivo Verification of C*c*-target Interactions: BiFC Assays

In an attempt to reduce the rate of false positives and corroborate *in vivo* the interactions between C*c* and its novel putative interaction partners identified in this work, BiFC was employed. This approach permits the analysis of protein-protein interactions in their biological environment, as well as the localization of the protein complexes [39]. For this purpose, C*c* was fused with the C-end fragment of the yellow fluorescent protein (cYFP), whereas its novel protein interaction partners, previously identified *in vitro*, were fused with the N-end fragment of the YFP (nYFP). In each case, coding cDNAs were cloned immediately before the corresponding YFP fragment. The HEK293T cells – rather than *Jurkat T* cells - were co-transfected due to their better efficiency of transient transfection and great adherence, so allowing one to monitor the changes in cell morphology and protein localization. The interaction of C*c* with its counterparts was followed by fluorescence, due to the YFP reconstitution upon C*c*-target binding (Figure 2).

cDNA coding for human C*c* and for 14 out of the 21 potential C*c* interaction partners previously identified through the proteomic approach were purchased (Source BioScience). As shown in Table S1 and Figure S4, C*c* and the cDNA of its targets were cloned into vectors containing the cYFP and nYFP, respectively [40].

Among the 21 C*c* targets, ATP5β, CCT2, NAP1L4 and RPS7 were discarded since they have not been described as apoptosis-related proteins. In addition, cDNAs encoding hnRNP L and RBBP7 were not available at Source BioScience or the cDNA could not be amplified using PCR. Moreover, Hsp90B1 was discarded since it has been described in the literature as an Apaf-1 target that does not make direct contact with C*c* [41].

YFP fragments are known to complement each other with low efficiency, yet still be sufficiently efficient to yield fluorescent complexes even in the absence of a specific interaction [42]. To ensure that the interactions involving C*c* were not the result of spontaneous YFP complementation, several precise controls were

designed based on the expression of two fusion proteins that, being expressed in the same cellular compartment, were unable to interact. These positive vectors, pBiFC-bJunYN155 and pBiFC-bFosYC155, and negative vectors, pBiFC-bJunYN155 and pBiFC-bFosΔZipYC155, were used as controls [33].

Apo-C*c* needs to be translocated from the cytosol to mitochondria, where the C*c* hemelyase assembles the heme cofactor leading to the formation of the holoprotein. HEK293T cells transfected with both the C*c*-cYFP vector and the empty nYFP vector (Figure 3A) showed a punctuate fluorescence pattern for the distribution of C*c* under homeostatic conditions, thereby highlighting its mitochondrial localization [38]. On the other hand, following the treatment of cells with CPT, the fluorescence pattern became diffuse, consistent with the release of C*c* from mitochondria into the cytoplasm (Figure 3B). The expression of the C*c*-cYFP fusion protein was confirmed by Western blot using a rabbit anti-EGFP polyclonal antibody (Figure 3C).

BiFC assays were carried out on 14 putative C*c*-interacting proteins identified through the proteomic approach. With the exception of CSNKIIβ, CORO1A, TUBB and MCM7 proteins, the interaction between C*c* and the remaining 10 targets were corroborated *in vivo* (Figure 2 and Table 1). Some of these interactions occur in the cytoplasm, such as those involving ALDOA, eIF2α, MCM6, HSPA5 and YWHAE, while others, such as those involving hnRNP C1/C2 and SET whose YFP fluorescence overlaps with DAPI staining, take place inside the nucleus. Finally, the complexes ANP32B-C*c*, NCL-C*c* and STRAP-C*c* display nucleo-cytoplasmic localization.

The lack of interaction between C*c* and CSNKIIβ as demonstrated by the absence of YFP fluorescence is also shown in Figure 2. Intriguingly, CSNKIIβ had been described as an *in vitro* C*c* interaction partner as early as in the 1970s [43,44]. However, such interaction was not detected *in vivo* with BiFC.

The transient expression of C*c* targets fused to nYFP in the BiFC assays was checked through immunoblotting with a rabbit anti-EGFP polyclonal antibody.

As illustrated in Figure 2, all constructs yielded a band of the expected molecular mass for each target.

To double-check that these protein partners are novel and specific of C*c*, additional BiFC measurements were performed with C*c* from *Arabidopsis thaliana* as human and plant C*c* are well-conserved hemeproteins with similar electrostatic potential surfaces. As can be seen in Figure S5, all the proteins herein shown to interact with human C*c* yield positive results with plant C*c* too, and all of them interact at the same cell compartment with human and plant C*c*. Altogether, these findings confirm the specificity of all these proteins for the C*c* species.

In Silico Modeling of the C*c* Complexes

To correlate structural data on the protein interaction partners with *in vivo* measurements and to determine the 3D structure of the C*c* complexes, a set of theoretical computations based on docking algorithms were performed [45]. For this purpose, either known structures, as deposited in the PDB database, or homology models were used to set the initial coordinates. In fact, the complexes involving ALDOA (4ALD.pdb) [46], ANP32B (2RR6.pdb) [47], eIF2α (1Q8K.pdb) [48], SET (2E50.pdb) [49] and YWHAE (2BR9.pdb) [50] and C*c* (1J3S.pdb) [51] were modeled using the PDB coordinates. The structure corresponding to STRAP was obtained by homology comparison using the MODELLER software [52]. In order to define the interface on C*c* involved in the interaction with its above-mentioned targets, soft docking calculations were performed using BIGGER [34]. The C*c*-complexes with the best global score values are shown in Figure 4. Interestingly, C*c* uses the same surface surrounding the heme crevice (Figure 4) to interact with all novel interaction partners as earlier studies have shown it to do with its physiological redox partners, namely cytochrome c_1 [53], cytochrome *c* peroxidase [54] and cytochrome *c* oxidase [55]. Figure 4 shows the distribution of mass centers for C*c* with respect to the protein interaction partners. Notably, all of them preferably explore a well-defined area of C*c*.

In vitro Validation of C*c* Adducts: SPR, NMR and ITC Measurements

The interaction between C*c* and its protein partners was measured by SPR, NMR and ITC experiments. For SPR spectroscopy, human C*c* was immobilized on the sensor surface. Six C*c* targets – ANP32B, eIF2α, hnRNP C1/C2, HSPA5, SET and YWHAE – were overexpressed as soluble recombinant proteins. The SPR sensograms of C*c*-binding to YWHAE, eIF2α, hnRNP C1/C2, HSPA5 and SET are shown in Figure 5, in which the background response was subtracted from the sample sensogram to obtain the actual binding response. The background response was recorded by injecting the analyte through a control or reference flow cell which has no ligand immobilized on the sensor surface. The C*c*-ANP32B interaction could not be detected by this technique.

The interactions of C*c* with a total of six soluble targets were further analyzed in solution by NMR and ITC. Figure 6 shows details of the ^{15}N-HSQC spectra of C*c* upon binding to eIF2α, ANP32B, HSPA5, SET, YWHAE and hnRNP C1/C2. Noteworthy, significant CSPs in several C*c* amide signals – in particular, in that corresponding to the residue glutamate 89 – were observed upon binding of C*c* to its partners, what is indicative for complex formation in solution of C*c* with all but one (hnRNP C1/C2) of the partners. Also, some C*c* amide signals broaden beyond the detection limit, thereby suggesting the formation of a long-lived complex, with lifetimes substantially large (in the range of seconds), between C*c* and its targets, as inferred from SPR measurements. Furthermore, the ITC thermograms and isotherms revealed that C*c* binds to its nucleo/cytoplasmic targets herein reported (Figure 7) – except for hnRNP C1/C2 – with a higher affinity (dissociation constant ranging between 1 and 5 μM) than to its mitochondrial redox targets. Interestingly, ANP32B, whose binding to C*c* was not detected by SPR, specifically interacted with C*c* when analyzed by NMR and ITC (Table 1). Altogether these structural and functional data suggest that these complexes are highly specific and mainly involve the surface of C*c* surrounding the heme cleft, except for the C*c*-SET complex in which additional residues placed at the opposite face of the heme group are also perturbed

(Figure 8). In the latter complex, C*c* might be localized in between the two subunits of the SET dimer so as to extend the C*c*-interacting surface. Figure 8 shows not only how relevant the electrostatic interactions are in bringing both proteins sufficiently close to each other but also how relevant the hydrophobic contacts are to stabilize a well-defined orientation. Moreover, C*c* yields not only specific but also much more stable complexes with its new apoptotic targets as compared with those previously described for its well-known respiratory partners (i.e. cytochrome bc_1 and cytochrome *c* oxidase of the mitochondrial electron transfer chain, with lifetimes of ca. 5 and 1 ms, respectively) [56,57].

Network of the Novel C*c*-Partner Interactions

In this study, human C*c* has been identified as a promiscuous protein, able to interact with at least 8 confirmed protein targets (Table 1) following its release from mitochondria into the cytosol during apoptosis. Thus, C*c* appears to be part of a complex regulatory network (Figure 9).

Figure 9 organizes the main functions of these novel C*c* interaction partners in a diagram divided into five main categories:

1. DNA Repair

The SET complex is constituted by SET, pp32, HMG-2, Ape1, NM23-H1 and TREX1 (Figure 9B) [58]. Under homeostatic conditions, this complex is associated with the endoplasmic reticulum (ER), but is mobilized in the nucleus in response to oxidative stress [59]. In fact, Ape1, and possibly TREX1 and NM23-H1, seem to be involved in the base excision repair mechanism for single-stranded DNA nicks [60] appearing with oxidative stress [61].

DNA double-strand breaks are generated by exogenous factors – topoisomerase inhibitors like CPT – and also during DNA replication. Mechanisms to detect DNA breaks and trigger DNA repair pathways as well as cell cycle checkpoints have evolved in cells [62,63]. hnRNP C1/C2 has been demonstrated to bind to chromatin in a DNA-damage-dependent manner, as well as to play a role in DNA repair and/or damage response (Figure 9) [64].

2. Cell Survival Pathways

14-3-3 proteins are involved in the regulation of a wide range of cellular processes, such as the inflammatory response, mitogenic and cell survival signaling, the cell cycle, transcriptional activity, DNA replication, DNA damage and apoptosis [65]. 14-3-3 epsilon (YWHAE), a cytoplasmic member of the family (Figure 9), has been involved in the regulation of multiple cell survival signaling pathways such as TNF-α/NF-κβ [65,66] and PI-3K/AKT [67].

STRAP (serine-threonine kinase receptor-associated protein) has been identified as a partner of PDK1 [68]. In this study, the co-expression of PDK1 and STRAP suppresses apoptotic cell death. These results suggest that STRAP plays an important role in the modulation of the PDK1-mediated survival signaling pathway. Indeed, STRAP not only positively regulates PDK1, but also regulates the activity of PDK1 downstream targets, activating AKT and inhibiting Bad [69] and thereby promoting cell survival.

While HSPA5 is mainly found in the endoplasmic reticulum (ER), it is also in the cytoplasm, the nucleus and on the cell surface [70,71,72]. During ER stress, HSPA5 is released from ER into the cytoplasm, interacting with the IKK complex [73] and promoting cell survival and cell proliferation through the NF-κβ signaling pathway (Figure 9B). Furthermore, HSPA5 physically interacts with Raf-1, known to phosphorylate and inactivate Bad, which results in resistance to apoptosis [74], stabilizes the mitochondrial membrane permeability and inhibits ER stress-induced apoptosis [75].

Hsp70 (Heat shock protein 70) is known to protect cells from apoptosis induced by heat shock, tumor necrosis factor, growth factor withdrawal, oxidative stress and radiation [76,77]. Recently, NCL has been shown to act as a downstream effector of Hsp70 in protecting cells against oxidative stress-induced apoptosis [78].

3. Metabolic Pathways Blocked During Apoptosis

The inhibition of protein synthesis enhances apoptosis through different stimuli [79]. Under apoptotic conditions, eIF2α has been shown to be phosphorylated by PKR. Post-translational modified eIF2α seems to inhibit translation during apoptosis [80] and to be an essential step for autophagy initiation [81].

4. Caspase Inhibition

ANP32B (Acidic leucine-rich Nuclear Phosphoprotein 32 B) is involved in gene regulation, acting as a histone chaperone [47] or modulating mRNA trafficking as a HuR ligand [82]. In addition, ANP32B can act as a caspase-3 inhibitor (Figure 9B) since the expression of endogenous ANP32B blocked by a specific siRNA enhances caspase-3 activation and promotes apoptosis [82]. On the other hand, ANP32B overexpression results in the rescue of Rat1 cells from induced apoptosis [83].

ALDOA (Aldolase A) is involved in the conversion of fructose-1, 6-bisphosphate to dihydroxyacetonephosphate and glyceraldehyde-3-phosphate [84]. The role of glyceraldehyde-3-phosphate as a reversible and non-competitive inhibitor of caspase-3 has been recently proposed (Figure 9B) [85].

The ER chaperone protein, GRP78 (HSPA5), is involved in the folding and assembly of proteins in the ER [86]. Its synthesis can be stimulated by stress conditions that perturb ER function and calcium homeostasis [87]. In fact, a subpopulation of HSPA5 exists as an ER transmembrane protein blocking caspase-7 activation (Figure 9B). Furthermore, HSPA5 forms an inhibitory complex along with caspase-12 (Figure 9B), preventing its release from the ER [88] and blocking apoptosis.

5. Inhibition of Apoptotic Pathways

Apart from the role of YWHAE and STRAP as positive regulators of cell survival pathways, both are involved in the inhibition of apoptotic signaling pathways through the sequestering of pro-apoptotic proteins (Figure 9B). Whereas YWHAE interacts with Bad [89,90], PKC [91] and Ask1 [92], STRAP synergizes with Smad7 in the inhibition of TGF-β signaling, thus blocking apoptosis [93,94].

Moreover, a novel inhibitory function for STRAP regarding Ask1-induced apoptosis has recently been proposed [95].

The three nucleases – Ape1, NM23-H1 and TREX1 – which form the SET complex are activated during PCD by the cleavage of the inhibitor protein SET by granzyme A or K, causing single-stranded DNA damage [61,96,97].

DISCUSSION

In vivo functions displayed by known components of apoptotic signaling pathways such as Bcl-2 proteins, caspases and Apaf-1 have been defined by genetic analyses [2]. However, this approach has hardly been used in the case of C*c* due to its essential requirement during mitochondrial respiration, with the exception of two reports leading to different conclusions [21,98]. In Li *et al.* [98], a C*c* knockout cell line was obtained that showed resistance to inducers for the apoptotic intrinsic pathway, but an increased sensitivity to extrinsic ones. However, Vempati *et al.* [21] indicated that the C*c* knockout cell line developed by Li's group expressed a testis-specific C*c* isoform. They then removed both C*c* isoforms and observed that the cell line was resistant to both apoptotic intrinsic and extrinsic pathway inducers.

Cell fate is known to be regulated by a fine-tuned balance between pro-apoptotic and pro-survival signaling pathways. The data obtained in this study reveals the interaction of human C*c* with eight novel partners, extensively considered as pro-survival, anti-apoptotic proteins (Figure 9). Some of the novel C*c* interaction partners identified in the study are involved in DNA damage response/repair mechanisms, protein synthesis, survival signaling pathways and processes known to be essential during homeostatic cell growth. Other C*c* targets block apoptosis by inhibiting caspases or impairing apoptotic signals. It is worth mentioning that some of these novel C*c* counterparts – namely, SET, YWHAE, STRAP and HSPA5 – act either in cell survival or in apoptosis.

Intriguingly, C*c* offers the surface surrounding the heme pocket for interaction with all partners reported in this study, as inferred from the docking calculations.

In fact, the area matches that used by C*c* to bind the vast majority of its known redox partners [53,54,99-102]. The *in vitro* interactions of some of these C*c* complexes, namely those involving eIF2α, hnRNP C1/C2, ANP32B, HSPA5, SET and YWHAE have been mostly corroborated by combining SPR, NMR and ITC approaches (Figures 5-8). These measurements reveal that the bimolecular complexes formed by C*c* with all its novel nuclear or cytoplasmic targets are specific and rather stable, as is the well-known interaction of C*c* with Apaf-1 to form the apoptosome (Figure 8). Interestingly, the surface used by C*c* (mainly residues surrounding the heme cleft) to bind to Apaf-1 and to the novel counterparts herein reported is very similar, and resembles that reported for the well-known C*c*-involving electron transfer complexes. Unlike such novel stable complexes, the redox interactions of mitochondrial C*c* with cytochrome bc_1 or cytochrome *c* oxidase are transient and highly dynamic, as the electron transfer reactions do demand. This finding suggests that the balance between cell life and death is closely related to transient and stable protein-protein interactions, respectively.

The biointeractomic scaffold hovering around C*c* occurs in different cellular compartments, as indicated by BiFC assays (Figure 2). Along with the intrinsic apoptotic route that leads to apoptosome formation and caspase activation, C*c* interacts with other proteins located in the cytoplasm such as YWHAE, STRAP, ALDOA and eIF2α, as well as with those translocated to the cytoplasm after an apoptotic stimulus such as HSPA5. Notably, some nuclear protein targets of C*c* – namely hnRNP C1/C2, SET and ANP32B – have also been identified. All of these are involved in DNA damage response, DNA replication and transcriptional regulation. To the knowledge of the authors, the present study represents the first time that nuclear protein interaction partners of C*c* have been proposed, explaining the nuclear localization of the heme protein, as observed previously [12,13,103].

These new C*c*-interacting targets suggest additional functions for C*c* beyond electron transfer reaction inside the mitochondria and apoptosome formation under cytosolic PCD stimuli. C*c* might be key in a complex signaling network by

disrupting cell survival and unlocking apoptotic pathways. In support of this model, the *Drosophila* C*c* distal knockout mutant displays a profound delay of apoptosis, even if the heme protein is not essential for the assembly of an apoptosome-like structure [19,104].

Nevertheless, evidence for new targets and potential new functions ascribed to C*c* during apoptosis allows one to understand the different phenotypes of C*c* and Apaf-1 knockouts [21,22,23], which cannot be explained if C*c* is restricted to bind Apaf-1 during apoptosis. In contrast, both phenotypes could be easily harmonized if C*c* plays a broader and crucial role as a PCD signaler, unlocking apoptosis and inhibiting cell survival.

In summary, the present study suggests a multifunctional action of C*c* in response to PCD stimuli. The findings can open up new ways to understand the process in organisms which lack Apaf-1 or whose apoptosome is devoid of C*c*. Given that C*c* is highly concentrated in the mitochondrial intermembrane space and that its release into the cytoplasm is an evolutionarily well-conserved event, it is likely that C*c* regulates other metabolic processes during PCD, as has been similarly corroborated in plants [105].

ACKNOWLEDGEMENTS

The authors wish to thank Dr. R. Rodríguez (cicCartuja, Seville, Spain) for her contribution to mass spectrometry analysis and Dr. A. Orea (cicCartuja, Seville, Spain) for her support with fluorescence microscopy. nYFP and cYFP vectors were kindly provided by Dr. P. Ciruela (Barcelona, Spain) and positive and negative controls – pBiFC-bJunYN155, pBiFC-bFosYC155 and pBiFC-bFosΔZipYC155 – for BiFC assays were kindly offered by Dr. T.K. Kerppola (Ann Arbor, Michigan, USA). The proteomic analyses were carried out at the "Proteomics Facility UCM-FPCM', a member of the ProteoRed Network". The authors are grateful to both the Spanish Ministry of Science and Innovation (BFU2009-07190 and BFU2012-31670) and the Regional Government of Andalusia (BIO198) for their financial support. Additional funding for J. Martínez-Fábregas was provided by a Spanish Ministry of Science and Innovation FPI grant (BES-2007-16156). Support for the recording of SPR measurements at Saarland University (Saarbrücken, Germany) was provided to K. González-Arzola through an IUBMB Wood-Whelan Fellowship. The authors wish to thank Blas Moreno-Beltrán for his critical reading of the manuscript.

REFERENCES

1. Jiang, X. and Wang, X. (2004). Cytochrome *c*-mediated apoptosis. Annu. Rev. Biochem. 73, 87-106.

2. Elmore, S. (2007). Apoptosis: A review of programmed cell death. Toxicol. Pathol. 35, 495-516.

3. Nuñez, G., Benedict, M.A., Hu, Y. and Inohara, N. (1998). Caspases: the proteases of the apoptotic pathway. Oncogene 17, 3237-3245.

4. Krammer, P.H. (2000). CD95's deadly mission in the immune system. Nature 407, 789-795.

5. Suen, D.F., Norris, K.L. and Youle, R.J. (2008). Mitochondrial dynamics and apoptosis. Genes Dev. 22, 1577-1590.

6. Chipuk, J.E. and Green, D.R. (2005). Do inducers of apoptosis trigger caspase-independent cell death? Nat. Rev. Mol. Cell Biol. 6, 268-275.

7. Yu, X., Acehan, D., Ménétret, J.F., Booth, C.R., Ludtke, S.J., Riedl, S.J., Shi, Y., Wang, X. and Akey, C.W. (2005). A structure of the human apoptosome at 12.8 Å resolution provides insights into this cell death platform. Structure 13, 1725-1735.

8. Li, P., Nijhawan, D., Budihardjo, I., Srinivasula, S.M., Ahmad, M., Alnemri, E.S. and Wang, X. (1997). Cytochrome *c* and dATP-dependent formation of Apaf-1/Caspase-9 complex initiates an apoptotic protease cascade. Cell 91, 479-489.

9. Forman, H.J. and Azzi, A. (1997). On the virtual existence of superoxide anions in mitochondria: thoughts regarding its role in pathophysiology. FASEB J. 11, 374-375.

10. Delivani, P. and Martin, S.J. (2006). Mitochondrial membrane remodeling in apoptosis: an inside story. Cell Death Differ. 13, 2007-2010.

11. Solary, E., Giordanetto, F. and Kroemer, G. (2008). Re-examining the role of cytochrome c in cell death. Nat. Genet. 40, 379-380.

12. Nur-E-Kamal, A., Gross, S.R., Pan, Z., Balklava, Z., Ma, J. and Liu, L.F. (2004). Nuclear translocation of cytochrome *c* during apoptosis. J. Biol. Chem. 279, 24911-24914.

13. Ruíz-Vela, A., González de Buitrago, G. and Martínez-A, C. (2002). Nuclear Apaf-1 and cytochrome *c* redistribution following stress-induced apoptosis. FEBS Lett. 517, 133-138.

14. Boehning, D., Patterson, R.L., Sedaghat, L., Glebova, N.O., Kurosaki, T. and Snyder, S.H. (2003). Cytochrome *c* binds to inositol (1,4,5) triphosphate receptors, amplifying calcium-dependent apoptosis. Nat. Cell Biol. 5 (12), 1051-1061.

15. Boehning, D., van Rossum, D.B., Patterson, R.L. and Snyder, S.H. (2005). A peptide inhibitor of cytochrome *c*/inositol 1,4,5-triphosphate receptor binding blocks intrinsic and extrinsic cell death pathways. Proc. Natl. Acad. Sci. USA 102, 1466-1471.

16. Szado, T., Vanderheyden, V., Parys, J.B., De Smedt, H., Rietdorf, K., Kotelevets, L., Chastre, E., Khan, F., Landegren, U., Söderberg, O., Bootman, M.D. and Roderick, H.L. (2008). Phosphorylation of inositol 1,4,5-triphosphate receptors by protein kinase B/Akt inhibits Ca^{2+} release and apoptosis. Proc. Natl. Acad. Sci. USA 105, 2427-2432.

17. Giannattasio, S., Atlante, A., Antonacci, L., Guaragnella, N., Lattanzio, P., Passarella, S. and Marra, E. (2008). Cytochrome *c* is released from coupled mitochondria of yeast en route to acetic acid-induced programmed cell death and can work as an electron donor and a ROS scavenger. FEBS Lett. 582, 1519-1525.

18. Balk, J., Leaver, C.J. and McCabe, P.F. (1999). Translocation of cytochrome *c* from the mitochondria to the cytosol occurs during heat-induced programmed cell death in cucumber plants. FEBS Lett. 463, 151-154.

19. Arama, E., Bader, M., Srivastava, M., Bergmann, A. and Steller, H. (2006). The two Drosophila cytochrome *c* proteins can function in both respiration and caspase activation. EMBO J. 25, 232-243.

20. Bossy-Wetzel, E., Newmeyer, D.D. and Green, D.R. (1998). Mitochondrial cytochrome c release in apoptosis occurs upstream of DEVD-specific caspase activation and independently of mitochondrial transmembrane depolarization. EMBO J. 17, 37-49.

21. Vempati, U.D., Diaz, F., Barrientos, A., Narisawa, S., Mian, A.M., Millán, J.L., Boise, L.H. and Moraes, C.T. (2007). Role of cytochrome *c* in apoptosis: increased sensitivity to tumor necrosis factor alpha is associated with respiratory defects but not with lack of cytochrome *c* release. Mol. Cell. Biol. 27, 1771-1783.

22. Marsden, V.S., O'Connor, L., O'Reilly, L.A., Silke, J., Metcalf, D., Ekert, P.G., Huang, D.C., Cecconi, F., Kuida, K., Tomaselli, K.J., Roy, S., Nicholson, D.W., Vaux, D.L., Bouillet, P., Adams, J.M. and Strasser, A. (2002). Apoptosis initiated by Bcl-2-regulated caspases activation independently of the cytochrome *c*/Apaf-1/caspases-9 apoptosome. Nature 419, 634-637.

23. Shawgo, M.E., Shelton, S.N. and Robertson, J.D. (2009). Caspase-9 activation by the apoptosome is not required for Fas-mediated apoptosis in type II Jurkat cells. J. Biol. Chem. 284, 33447-33455.

24. Hüttemann, M., Pecina, P., Rainbolt, M., Sanderson, T.H., Kagan, V.E., Samavati, L., Doan, J.W. and Lee, I. (2011). The multiple functions of cytochrome *c* and their regulation in life and death decisions of the mammalian cell: From respiration to apoptosis. Mitochondrion 11, 369-381.

25. Rodríguez-Roldán, V., García-Heredia, J.M., Navarro, J.A., Hervás, M., De la Cerda, B., Molina-Heredia, F.P. and De la Rosa, M.A. (2006). A comparative kinetic analysis of the reactivity of plant, horse and human cytochrome c towards cytochrome c oxidase. Biochem. Biophys. Res. Commun. 346, 1108-1113.

26. Johnson, N., Ng, T.T. and Parkin, J.M. (1997). Camptothecin causes cell cycle perturbations within T-lymphoblastoid cells followed by dose dependent induction of apoptosis. Leuk. Res. 21, 961-972.

27. Goldstein, J.C., Waterhouse, N.J., Juin, P., Evan, G.I. and Green, D.R. (2000). The coordinate release of cytochrome *c* during apoptosis is rapid, complete and kinetically invariant. Nat. Cell Biol. 2, 156-162.

28. Nicoletti, I., Migliorati, G., Pagliacci, M.C., Grignani, F. and Riccardi, C. (1991). A rapid and simple method for measuring thymocite apoptosis by propidium iodide staining and flow cytometry. J. Immunol. Methods 139, 271-279.

29. Liu, X., Kim, C.N., Yang, J., Jemmerson, R. and Wang, X. (1996). Induction of apoptotic program in cell-free extracts: requirement for dATP and cytochrome c. Cell 86, 147-157.

30. Azzi, A., Bill, K. and Broger, C. (1982). Affinity chromatography purification of cytochrome *c* binding enzymes. Proc. Natl. Acad. Sci. USA 79, 2447-2450.

31. Candiano, G., Bruschi, M., Musante, L., Santucci, L., Ghiggeri, G.M., Carnemolla, B., Orecchia, P., Zardi, L. and Righetti, P.G. (2004). Blue silver: a very sensitive colloidal Coomassie G-250 staining for proteome analysis. Electrophoresis 25, 1327-1333.

32. Sechi, S. and Chait, B.T. (1998). Modification of cysteine residues by alkylation. A tool in peptide mapping and protein identification. Anal. Chem. 70, 5150-5158.

33. Hu, C.D., Chinenov, Y. and Kerppola, T.K. (2002). Visualization of interactions among bZip and Rel family proteins in living cells using bimolecular fluorescence complementation. Mol. Cell 9, 789-798.

34. Palma, P.N., Krippahl, L., Wampler, J.E. and Moura, J.J. (2000). BiGGER: a new (soft) docking algorithm for predicting protein interactions. Proteins 39 (4), 372-384.

35. Olteanu, A., Patel, C.N., Dedmon, M.M., Kennedy, S., Linkoff, M.W., Minder, C.M., Potts, P.R., Deskmukh, M. and Pielak, G.J. (2003). Stability and apoptotic activity of recombinant human cytochrome c. Biochem. Biophys. Res. Commun. 312, 733-740.

36. Janocha, S., Bichet, A., Zöllner, A. and Bernhardt, R. (2011). Substitution of lysine with glutamic acid at position 193 in bovine CYP11A1 significantly affects protein oligomerization and solubility but not enzymatic activity. Biochem. Biophys. Acta 1814, 126-131.

37. Allen, J.W., Tomlinson, E.J., Hong, L. and Ferguson, S.J. (2002). The Escherichia coli cytochrome c maturation (Ccm) system does not detectably attach heme to single cysteine variants of an apopcytochrome c. J. Biol. Chem. 277, 33559-33563.

38. Goldstein, J.C., Muñoz-Pinedo, C., Ricci, J.E., Adams, S.R., Kelekar, A., Schuler, M., Tsien, R.Y. and Green, D.R. (2005). Cytochrome *c* is released in a single step during apoptosis. Cell Death Differ. 12, 453-462.

39. Hu, C.D., Grinberg, A.V. and Kerppola, T.K. (2006). Visualization of protein interactions in living cells using bimolecular fluorescence complementation (BiFC) analysis. Curr. Protoc. Cell Biol. (Chapter 21, Unit 21.3).

40. Gandia, J., Galino, J., Amaral, O.B., Soriano, A., Lluís, C., Franco, R. and Ciruela, F. (2008). Detection of higher-order G protein-coupled receptor oligomers by a combined BRET-BiFC technique. FEBS Lett. 582, 2979-2984.

41. Pandey, P., Saleh, A., Nakazawa, A., Kumar, S., Srinivasula, S.M., Kumar, V., Weichselbaum, R., Nalin, C., Alnemri, E.S., Kufe, D. and Kharbanda, S. (2000). Negative regulation of cytochrome c-mediated oligomerization of Apaf-1 and activation of procaspase-9 by heat shock protein 90. EMBO J. 19, 4310-4322.

42. Kerppola, T.K. (2006). Design and implementation of bimolecular fluorescence complementation (BiFC) assays for the visualization of protein interactions in living cells. Nat. Protoc. 1, 1278-1286.

43. Taborsky, G. (1970). Interaction of cytochrome *c* and the phosphoprotein phosvitin. Formation of a complex with an intact 695-m.mu. absorption band. Biochemistry 9, 3768-3774.

44. Yoshimura, T., Matsushima, A. and Aki, K. (1979). Interaction of cytochrome *c* with the phosphoprotein phosvitin. Biochim. Biophys. Acta 581, 361-324.

45. Mintseris, J., Wiehe, K., Pierce, B., Anderson, R., Chen, R., Janin, J. and Weng, Z. (2005). Protein-protein docking benchmark 2.0: an update. Proteins 60, 214-216.

46. Dalby, A., Dauter, Z. and Littlechild, J.A. (1999). Crystal structure of human muscle aldolase complexed with fructose 1,6-bisphosphate: mechanistic implications. Protein Sci. 8, 291-297.

47. Tochio, N., Umehara, T., Munemasa, Y., Suzuki, T., Sato, S., Tsuda, K., Koshiba, S., Kigawa, T., Nagai, R. and Yokoyama, S. (2010). Solution structure of histone chaperone ANP32B: interaction with core histones H3-H4 through its acidis concave domain. J. Mol. Biol. 401, 97-114.

48. Ito, T., Marintchev, A. and Wagner, G. (2004). Solution structure of human initiation factor eIF2alpha reveals homology to the elongation factor eEF1B. Structure 12, 1693-1704.

49. Muto, S., Senda, M., Akai, Y., Sato, L., Suzuki, T., Nagai, R., Senda, T. and Horikoshi, M. (2007). Relationship between the structure of SET/TAF-Iβ/INHAT and its histone chaperone activity. Proc. Natl. Acad. Sci. USA 104, 4285-4290.

50. Yang, X., Lee, H.W., Sobott, F., Papagrigoriou, E., Robinson, C.V., Grossmans, J.G., Sundström, M., Doyle, D.A. and Elkins, J.M. (2006). Structural basis for protein-protein interactions in the 14-3-3 protein family. Proc. Natl. Acad. Sci. USA 103, 17237-17242.

51. Jeng, W.Y., Shiu, J.H., Tsai, Y.H. and Chiang, W.J. (2003). Solution structure of reduced recombinant human cytochrome *c.* Doi: 10.2210/pdb1j3s/pdb

52. Dolan, M.A., Noah, J.W. and Hurt, D. (2012) Comparison of common homology modelling algorithms: application of user-defined alignments. Methods Mol. Biol. 857, 399-414.

53. König, B.W., Osheroff, N., Wilms, J., Muijsers, A.O., Dekker, H.L. and Margoliash, E. (1980). Mapping of the interaction domain for purified cytochrome *c1* on cytochrome *c*. FEBS Lett. 111, 395-398.

54. Worrall, J.A., Kolczak, U., Canters, G.W. and Ubbink, M. (2001). Interaction of yeast iso-1-cytochrome *c* with cytochrome *c* peroxidase investigated by [15N, 1H] heteronuclear NMR spectroscopy. Biochemistry 40, 7069-7076.

55. Sakamoto, K., Kamiya, M., Imai, M., Shinzawa-Itoh, K., Uchida, T., Kawano, K., Yoshikawa, S. and Ishimori, K. (2011). NMR basis for interprotein electron transfer gating between cytochrome *c* and cytochrome *c* oxidase. Proc. Natl. Acad. Sci. USA 108, 12271-12276.

56. Lange, C. and Hunte, C. (2002). Crystal structure of the yeast cytochrome bc_1 complex with its bound substrate cytochrome *c*. Proc. Natl. Acad. Sci. USA 99, 2800-2805.

57. Li, Y., Naqui, A., Frey, T.G. and Chance, B. (1987). A new procedure for the purification of monodisperse highly active cytochrome *c* oxidase from bovine heart. Biochem. J. 242, 417-423.

58. Yan, N., Regalado-Magdos, A.D., Stiggelbout, B., Lee-Kirsch, M.A. and Lieberman, J. (2010). The cytosolic exonuclease TREX1 inhibits the innate immune response to human immunodeficiency virus type 1. Nat. Immunol. 11, 1005-1013.

59. Martinvalet, D., Zu, P. and Lieberman, J. (2005). Granzyme A induces caspase-independent mitochondrial damage, a required first step for apoptosis. Immunity 22, 355-370.

60. Demple, B. and DeMott, M.S. (2002). Dynamics and diversions in base excision DNA repair of oxidized abasic lesions. Oncogene 21, 8926-8934.

61. Chowdhury, D., Beresford, P.J., Zhu, P., Zhang, D., Sung, J.S., Demple, B., Perrino, F.W. and Lieberman, J. (2006). The exonuclease TREX1 is in the SET complex and acts in concert with NM23-H1 to degrade DNA during granzyme A-mediated cell death. Mol. Cell 23, 133-142.

62. Sancar, A., Lindsey-Boltz, L.A., Unsal-Kaçmaz, K. and Linn, S. (2004). Molecular mechanisms of mammalian DNA repair and the DNA damage checkpoints. Annu. Rev. Biochem. 73, 39-85.

63. Jackson, S.P. (2002). Sensing and repairing DNA double-strand breaks. Carcinogenesis 23, 687-696.

64. Lee, S.Y., Park, J.H., Kim, S., Park, E.J., Yun, Y. and Kwon, J. (2005). A proteomics approach for the identification of nucleophosmin and heterogeneous nuclear ribonucleoprotein C1/C2 as chromatin-binding proteins in response to DNA double-strand breaks. Biochem. J. 388, 7-15.

65. Zuo, S., Xue, Y., Tang, S., Yao, J., Du, R., Yang, P. and Chen, X. (2010). 14-3-3 epsilon dynamically interacts with key components of mitogen-activated protein kinase signal module for selective modulation of the TNF-α-induced time course-dependent NF-κβ activity. J. Proteome Res. 9, 3465-3478.

66. Franzoso, G., Zazzeroni, F. and Papa, S. (2003). JNK: a killer on a transcriptional leash. Cell Death Differ. 10, 13-15.

67. Tzivion, G., Gupta, V.S., Kaplun, L. and Balan, V. (2006). 14-3-3 proteins as potential oncogenes. Semin. Cancer Biol. 16, 203-213.

68. Seong, H.A., Jung, H., Choi, H.S., Kim, K.T. and Ha, H. (2005). Regulation of transforming growth factor-β signaling and PDK1 kinase activity by physical interaction between PDK1 and serine-threonine kinase receptor-associated protein. J. Biol. Chem. 280, 42897-42908.

69. Chen, Y., Rodrik, V. and Foster, D.A. (2005). Alternative phospholipase D/mTOR survival signal in human breast cancer cells. Oncogene 24, 672-679.

70. Mintz, P.J., Kim, J., Do, K.A., Wang, X., Zinner, R.G., Cristofanilli, M., Arap, M.A., Hong, W.K., Troncoso, P., Logothetis, C.J., Pasqualini, R. and Arap, W. (2003). Fingerprinting the circulating repertoire of antibodies from cancer patients. Nat. Biotechnol. 21, 57-63.

71. Shin, B.K., Wang, H., Yim, A.M., Le Naour, F., Brichory, F., Jang, J.H., Zhao, R., Puravs, E., Tra, J., Michael, C.W., Misek, D.E. and Hanash, S.M. (2003). Global profiling of the cell surface proteome of cancer cells uncovers an abundance of proteins with chaperone function. J. Biol. Chem. 278, 7607-7616.

72. Bukau, B. and Horwich, A.L. (1998). The Hsp70 and Hsp60 chaperone machines. Cell 92, 351-366.

73. Shkoda, A., Ruiz, P.A., Daniel, H., Kim, S.C., Rogler, G., Sartor, R.B. and Haller, D. (2007). Interleukin-10 blocked endoplasmic reticulum stress in intestinal epithelial cells: impact on chronic inflammation. Gastroenterology 132, 190-207.

74. Jin, S., Zhuo, Y., Guo, W. and Field, J. (2005). p21-activated kinase 1 (Pak1)-dependent phosphorylation of Raf-1 regulates its mitochondrial localization, phosphorylation of BAD, and Bcl-2 association. J. Biol. Chem. 280, 24698-24705.

75. Shu, C.W., Sun, F.C., Cho, J.H., Lin, C.C., Liu, P.F., Chen, P.Y., Chang, M.D., Fu, H.W. and Lai, Y.K. (2007). GRP78 and Raf-1 cooperatively confer resistance to endoplasmic reticulum stress-induced apoptosis. J. Cell Physiol. 215, 627-635.

76. Arya, R., Mallik, M. and Lakhotia, S.C. (2007). Heat shock genes – integrating cell survival and death. J. Biosci. 32, 595-610.

77. Zhao, Y., Wang, W. and Qian, L. (2007). Hsp70 may protect cardiomyocytes from stress-induced injury by inhibiting Fas-mediated apoptosis. Cell Stress Chap. 12, 83-95.

78. Jiang, B., Zhang, B., Liang, P., Song, J., Deng, H., Tu, Z., Deng, G. and Xiao, X. (2010). Nucleolin/C23 mediates the antiapoptotic effect of heat shock protein 70 during oxidative stress. FEBS J. 277, 642-652.

79. Polunovsky, V.A., Wendt, C.H., Ingbar, D.H., Peterson, M.S. and Bitterman, P.B. (1994). Induction of endothelial cell apoptosis by TNF-α: modulation by inhibitors of protein synthesis. Exp. Cell Res. 214, 584-594.

80. Saelens, X., Kalai, M. and Vandenabeele, P. (2001). Translation inhibition in apoptosis: Caspase-dependent PKR activation and eIF2-α phosphorylation. J. Biol. Chem. 276, 41620-41628.

81. Kouroku, Y., Fujita, E., Tanida, I., Ueno, T., Isoai, A., Kumagai, H., Ogawa, S., Kaufman, R.J., Kominami, E. and Momoi, T. (2007). ER stress (PERK/eIF2-α phosphorylation) mediates the polyglutamine-induced LC3 conversion, an essential step for autophagy formation. Cell Death Differ. 14, 230-239.

82. Shen, S.M., Yu, Y., Wu, Y.L., Cheng, J.K., Wang, L.S. and Chen, G.Q. (2010). Downregulation of ANP32B, a novel substrate of caspase-3, enhances caspase-3 activation and apoptosis induction in myeloid leukemic cells. Carcinogenesis 31, 419-426.

83. Sun, W., Kimura, H., Hattori, N., Tanaka, S., Matsuyama, S. and Shiota, K. (2006). Proliferation related acidic leucine-rich protein PAL31 functions as a caspase-3 inhibitor. Biochem. Biophys. Res. Commun. 342, 817-823.

84. Yao, D.C., Tolan, D.R., Murray, M.F., Harris, D.J., Darras, B.T., Geva, A. and Neufeld, E.J. (2004). Hemolytic anemia and severe rhabdomyolysis caused by compound heterozygous mutations of the gene for erythrocyte/muscle isozyme of aldolase, ALDOA $^{(Arg303X/Cys338Tyr)}$. Blood 103, 2401-2403.

85. Jang, M., Kang, H.J., Lee, S.Y., Chung, S.J., Kang, S., Chi, S.W., Cho, S., Lee, S.C., Lee, C.K., Park, B.C., Bae, K.H. and Park, S.G. (2009). Glyceraldehyde-3-Phosphate, a glycolytic intermediate, plays a key role in controlling cell fate via inhibition of caspase activity. Mol. Cell 28, 559-563.

86. Hsu, W.C., Wang, H.K., Lee, L.C., Fung, H.C., Lin, J.C., Hsu, H.P., Wu, Y.R., Ro, L.S., Hu, F.J., Chang, Y.T, Chen, G.J. and Chen, C.M. (2008). Promoter polymorphisms modulating HSPA5 expression may increase susceptibility to Taiwanese Alzheimer's disease. J. Neural Transm. 115, 1537-1543.

87. Lee, A.S. (2001). The glucose-regulated proteins: stress induction and clinical applications. Trends Biochem. Sci. 26, 504-510.

88. Rao, R.V., Peel, A., Logvinova, A., del Rio, G., Hermel, E., Yokota, T., Goldsmith, P.C., Ellerby, L.M., Ellerby, H.M. and Bredesen, D.E. (2002). Coupling endoplasmic reticulum stress to the cell death program: role of the ER chaperone GRP78. FEBS Lett. 514, 122-128.

89. Won, J., Kim, D.Y., La, M., Kim, D., Meadows, G.G. and Joe, C.O. (2003). Cleavage of 14-3-3 protein by caspase-3 facilitates Bad interaction with Bcl-X(L) during apoptosis. J. Biol. Chem. 278, 19347-19351.

90. Zhang, L., Chen, J. and Fu, H. (1999). Suppression of apoptosis signal-regulating kinase 1-induced cell death by 14-3-3 proteins. Proc. Natl. Acad. Sci. USA 96, 8511-8515.

91. Supekova, L., Pezacki, J.P., Su, A.I., Loweth, C.J., Riedl, R., Geierstanger, B., Schultz, P.G. and Wemmer, D.E. (2002). Genomic effects of polyamide/DNA interactions on mRNA expression. Chem. Biol. 9, 821-827.

92. Subramanian, R.R., Zhang, H., Wang, H., Ichijo, H., Miyashita, T. and Fu, H. (2004). Interaction of apoptosis signal-regulating kinase 1 with isoforms of 14-3-3 proteins. Exp. Cell Res. 294, 581-591.

93. Datta, P.K. and Moses, H.L. (2000). STRAP and Smad7 synergize in the inhibition of transforming growth factor β signaling. Mol. Cell Biol. 20, 3157-3167.

94. Kleeff, J., Ishiwata, T., Maruyama, H., Friess, H., Truong, P., Büchler, M.W., Falb, D. and Korc, M. (1999). The TGF-beta signaling inhibitor Smad7 enhances tumorigenicity in pancreatic cancer. Oncogene 18, 5363-5372.

95. Jung, H., Seong, H.A., Manoharan, R. and Ha, H. (2010). Serine-threonine kinase receptor-associated protein inhibitis apoptosis signal-regulating kinase 1 function through direct interaction. J. Biol. Chem. 285, 54-70.

96. Fan, Z., Beresford, P.J., Oh, D.Y., Zhang, D. and Lieberman, J. (2003). Tumor suppressor NM23-H1 is a granzyme A-activated DNase during CTL-mediated apoptosis, and the nucleosome assembly protein SET is its inhibitor. Cell 112, 659-672.

97. Zhao, T., Zhang, H., Guo, Y., Zhang, Q., Hua, G., Lu, H., Hou, Q., Liu, H. and Fan, Z. (2007). Granzyme K cleaves the nucleosome assembly protein SET to induce single-stranded DNA nicks of target cells. Cell Death Differ. 14, 489-499.

98. Li, K., Li, Y., Shelton, J.M., Richardson, J.A., Spencer, E., Chan, Z.J., Wang, X. and Williams, R.S. (2000). Cytochrome *c* deficiency causes embryonic lethality and attenuates stress-induced apoptosis. Cell 12, 389-399.

99. Crowley, P.B., Rabe, K.S., Worrall, J.A., Canters, G.W. and Ubbink, M. (2002). The ternary complex of cytochrome *f* and cytochrome *c*: identification of a second binding site and competition for plastocyanin binding. Chembiochem. 3, 526-533.

100. Worrall, J.A., Reinle, W., Bernhardt, R. and Ubbink, M. (2003).Transient protein interactions studied by NMR spectroscopy: the case of cytochrome *c* and adrenodoxin. Biochemistry 42, 7068-7076.

101. Ubbink, M. and Bendall, D.S. (1997). Complex of plastocyanin and cytochrome c characterized by NMR chemical shift analysis. Biochemistry 36, 6326-6335.

102. Volkov, A.N., Ferrari, D., Worrall, J.A., Bonvin, A.M. and Ubbink, M. (2005). The orientations of cytochrome c in the highly dynamic complex with cytochrome b5 visualized by NMR and docking using HADDOCK. Protein Sci. 14, 799-811.

103. Godoy, L.C., Muñoz-Pinedo, C., Castro, L., Cardaci, S., Schonhoff, C.M., King, M., Tórtora, V., Marín, M., Miao, Q., Jiang, J.F., Kapralov, A., Jemmerson, R., Silkstone, G.G., Patel, J.N., Evans, J.E., Wilson, M.T., Green, D.R., Kagan, V.E., Radi, R. and Mannick, J.B. (2009). Disruption of the M80-Fe ligation stimulates the translocation of cytochrome *c* to the cytoplasm and nucleus in nonapoptotic cells. Proc. Natl. Acad. Sci. USA 106, 2653-2658.

104. Mendes, C.S., Arama, E., Brown, S., Scherr, H., Srivastava, M., Bergman, A., Steller, H. and Mollereau, B. (2006). Cytochrome *c*-d regulates developmental apoptosis in the Drosophila retina. EMBO Rep. 7, 933-939.

105. Martínez-Fabregas, J., Díaz-Moreno, I., González-Arzola K., Janocha, S., Navarro, J.A., Hervás, M., Bernhardt, R., Díaz-Quintana, A., and De la Rosa, M.A. (2013). New *Arabidopsis thaliana* cytochrome *c* partners: A look into the elusive role of cytochrome *c* in programmed cell death in plants. Mol. Cell. Proteomics 12, 3666-3676.

FIGURE LEGENDS

Figure 1. Proteomic workflow and 2D SDS-PAGE.

Left. Scheme of the proteomic workflow used to identify C*c*-interacting proteins. C*c* interaction partners were purified from untreated and CPT-treated Jurkat T cell extracts with affinity chromatography, using a column with the E104C mutant covalently bound to the thiol-sepharose matrix (C*c* TS-4B). Samples were resolved by 2D SDS-PAGE, with the resulting spots later being identified by MALDI-TOF/TOF. As controls, untreated and CPT-treated cell extracts were loaded into a blank column containing the sepharose matrix devoid of E104C (Blank TS-4B).

Right. Master gel calculated from the image analysis of gels run under different experimental conditions using the PDQuest software (see Supplemental Data). Red circles represent proteins identified under either apoptotic stimuli or homeostatic and apoptotic conditions. Such proteins are only retained in the C*c*-bounded TS-4B column, but not in the TS-4B column. Spot numbers are named in Table S2.

Figure 2. BiFC assays and Western blots showing the *in vivo* interaction of C*c* with its potential protein partners.

HEK293T cells were transfected with the C*c*-cYFP vector, along with another vector containing the N-terminal YFP fragment (nYFP) bound to each C*c* protein interaction partner. Images were captured 24 h after transient transfection with Lipofectamine 2000 (Invitrogen) and after 6 h of treatment with 10 μM CPT. Reconstruction of eYFP leads to the obtainment of fluorescence signal emission, indicative of interaction between C*c* and its partners. Positive and negative controls were used, as described by Hu *et al*. [39]. Scale bar is 5 μm. The expression of C*c* interaction partners fused to the nYFP fragment was determined by immunoblotting with a rabbit anti-EGFP polyclonal antibody (BioVision). No bands were observed in the Western blots with non-transfected cells (data not shown).

Figure 3. Location of cYFP tagged C*c* under normal and apoptotic conditions.

(A) Homeostatic conditions. Punctuate fluorescence pattern showing the mitochondrial distribution of C*c* into HEK293T cells co-transfected with the C*c*-cYFP vector and the empty nYFP vector using Lipofectamine 2000 (Invitrogen).

(B) Apoptotic conditions. Diffuse fluorescence pattern showing the cytoplasmic C*c* localization of C*c* in HEK293T cells transfected as in (A), but after 6 h of treatment with 10 μM CPT.

(C) Expression of C*c*-cYFP in HEK293T cells. Left panel, cells transfected with the C*c*-cYFP vector. Right panel, non-transfected cells. The C*c*-cYFP fusion protein was immunodetected by Western blot with an anti-EGFP antibody (BioVision).

Figure 4. Molecular docking models of C*c* complexes.

A) C*c*xALDOA docking model with the best global score value (left) in the ratio 1:1 and centers of mass distribution of 50 molecules of C*c* with respect to ALDOA (right). Ribbon representation of C*c* in magenta, with its heme group in white. The ribbon of ALDOA is colored in cyan.

B) C*c*xANP32B docking model with the best global score values (left) and centers of mass distribution of 50 molecules of C*c* with respect to ANP32B (right). Same color-coding as in (A).

C) C*c*xeIF2α docking model with the best global score values (left) and centers of mass distribution of 50 molecules of C*c* with respect to eIF2α (right). Same color-coding as in (A).

D) C*c*xSET docking model with the best global score values (left) and centers of mass distribution of 50 molecules of C*c* with respect to SET (right). Same color-coding as in (A).

E) C*c*xSTRAP docking model with the best global score values (left) and centers of mass distribution of 50 molecules of C*c* with respect to STRAP (right). Same color-coding as in (A).

F) C*c*xYWHAE docking model with the best global score values (left) and centers of mass distribution of 50 molecules of C*c* with respect to YWHAE (right). Same color-coding as in (A).

Figure 5. SPR measurements.

A) Sensograms recorded for the binding of human C*c* with eIF2α. Three replicate injections were performed for each protein concentration. In each sensogram, the signals from the control surface were subtracted.

B) As in (A), but for human C*c*-hnRNP C1/C2 complex.

C) As in (A), but for human C*c*-HSPA5 complex.

D) As in (A), but for human C*c*-SET complex.

E) As in (A), but for human C*c*-YWHAE complex.

Figure 6. CSPs and line-width of the glutamate 89 amide signal in reduced C*c* upon binding to its novel protein partners, as observed by NMR spectroscopy.

Details of the superimposed ^{15}N-HSQC spectra of ^{15}N-labeled C*c*, either free (blue) or upon binding to eiF2α, ANP32B, HSPA5, SET, YWHAE and hnRNP C1/C2 (red). In all cases, the C*c*:partner ratio was 1:1. The arrows indicate the direction and magnitude of CSPs.

Figure 7. ITC titrations of reduced C*c* with its protein partners.

The thermograms and binding isotherms (*top* and *bottom*, respectively) of C*c* with eiF2α, ANP32B, HSPA5, SET, YWHAE and hnRNP C1/C2 are shown. Standard errors are 5–10%.

Figure 8. Mapping of C*c* upon binding to its well-known and novel targets. C*c* residues at the interface area within the corresponding complexes are colored as follows: polar and charged residues in blue, hydrophobic residues in orange. The heme group is marked in green and the non-interacting residues in gray. Two 180º-rotated surface representations (*upper* and *lower*) are depicted for each complex. The horizontal color bars represent the stability and lifetime of the complexes, from highly dynamic/transient (red) to more rigid/stable (blue). Surface representations were generated from the structure of human C*c* (PDB entry 1J3S [51]). C*c* interfacial residues in the complex with Apaf-1, cytochrome *c* oxidase and cytochrome bc_1 were taken from references 7, 55 and 56, respectively.

Figure 9. Main functions ascribed to the novel C*c* protein partners and network of the resulting interactions.

(A) Diagram with the main functions of novel C*c* protein interaction partners identified *in vitro* through proteomics and confirmed *in vivo* through BiFC. All targets have been grouped into five functional categories. Several functions can be shared by the same target.

(B) Mapping the interactions between C*c* and its novel protein interaction partners, as well as of the latter with the proteins involved in cell death, proliferation and/or survival, as reported in the literature. Color-coding is the same as in (A).

Table 1. Human C*c* novel confirmed protein targets validated by different orthogonal approaches.

Protein Name	Protein Abbreviation	SDS-Page & MALDI-TOF/TOF MS	BiFC	Molecular Docking	SPR	NMR	ITC
Casein kinase II subunit beta	CSNKIIβ	+	-				
Chaperonin containing TCP1 subunit 2	CCT2	+	**nd[1]**				
Coronin-like protein	CORO1A	+	-				
Eukaryotic translation initiation factor 2 alpha*	eiF2α	+	+	+	+	+	+
Fructose 1,6-bisphosphate aldolase A*	ALDOA	+	+	+	**nd[4]**	**nd[4]**	**nd[4]**
Ribosomal protein S7	RPS7	+	**nd[1]**				
Tubulin beta chain	TUBB	+	-				
Tumor rejection antigen 1	Hsp90B1	+	**nd[2]**				
14-3-3 epsilon*	YWHAE	+	+	+	+	+	+
Heterogeneus nuclear ribonucleoprotein C1/C2*	hnRNP C1/C2	+	+	**nd[5]**	+	-	-
Histone-binding protein RBBP7	RBBP7	+	**nd[3]**	-	**nd[3]**	**nd[3]**	**nd[3]**
Minichromosome maintenance complex 6	MCM6	+	+	**nd[5]**	**nd[4]**	**nd[4]**	**nd[4]**
Minichromosome maintenance complex 7	MCM7	+	-				
SET nuclear oncogene*	SET	+	+	+	+	+	+
Acidic nuclear phosphoprotein 32B*	ANP32B	+	+	+	-	+	+
Heterogeneus nuclear ribonucleoprotein L	hnRNP L	+	**nd[3]**				
Nucleolin	NCL	+	+	**nd[5]**	**nd[4]**	**nd[4]**	**nd[4]**
Nucleosome assembly protein 1-like 4	NAP1L4	+	**nd[1]**				
Ser/Thr kinase receptor associated protein*	STRAP	+	+	+	**nd[4]**	**nd[4]**	**nd[4]**
ATP synthase subunit beta	ATP5β	+	**nd[1]**				
Heat shock 70 kDa protein*	HSPA5	+	+	**nd[5]**	+	+	+

nd[1]: not-determined because they are not apoptosis-related proteins; nd[2]: not-determined because the interaction with C*c* was previously discarded [41]; nd[3]: not-determined because their cDNAs were not available; nd[4]: not-determined because they were not overexpressed as soluble recombinant proteins; nd[5]: not-determined because their PDB coordinates were not available. Asterisk (*) stands for those C*c* protein interactors validated in at least 3 out of 6 techniques.

Figure 1

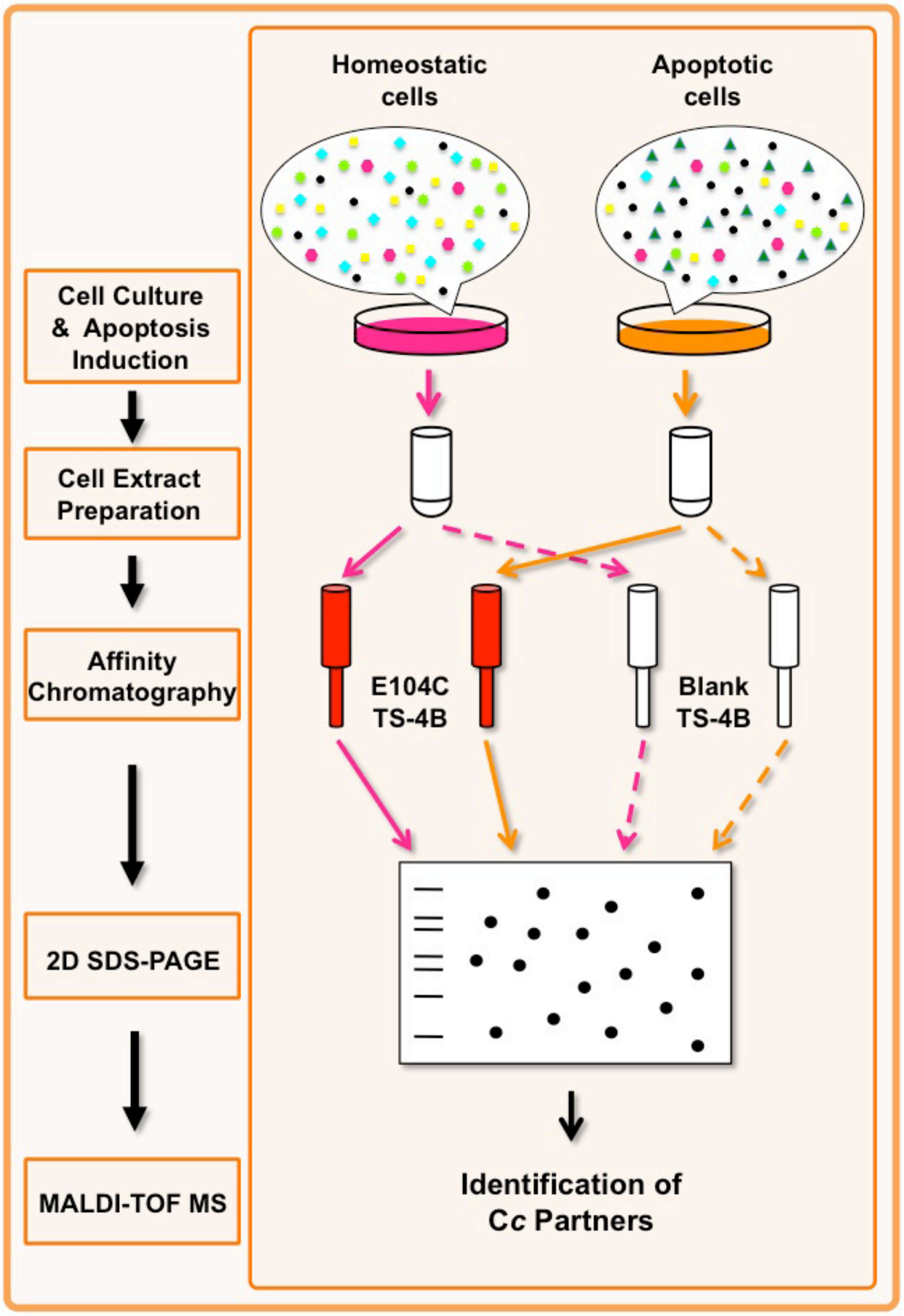
Homeostatic cells
Apoptotic cells
Cell Culture & Apoptosis Induction
Cell Extract Preparation
Affinity Chromatography
2D SDS-PAGE
MALDI-TOF MS
E104C TS-4B
Blank TS-4B
Identification of Cc Partners

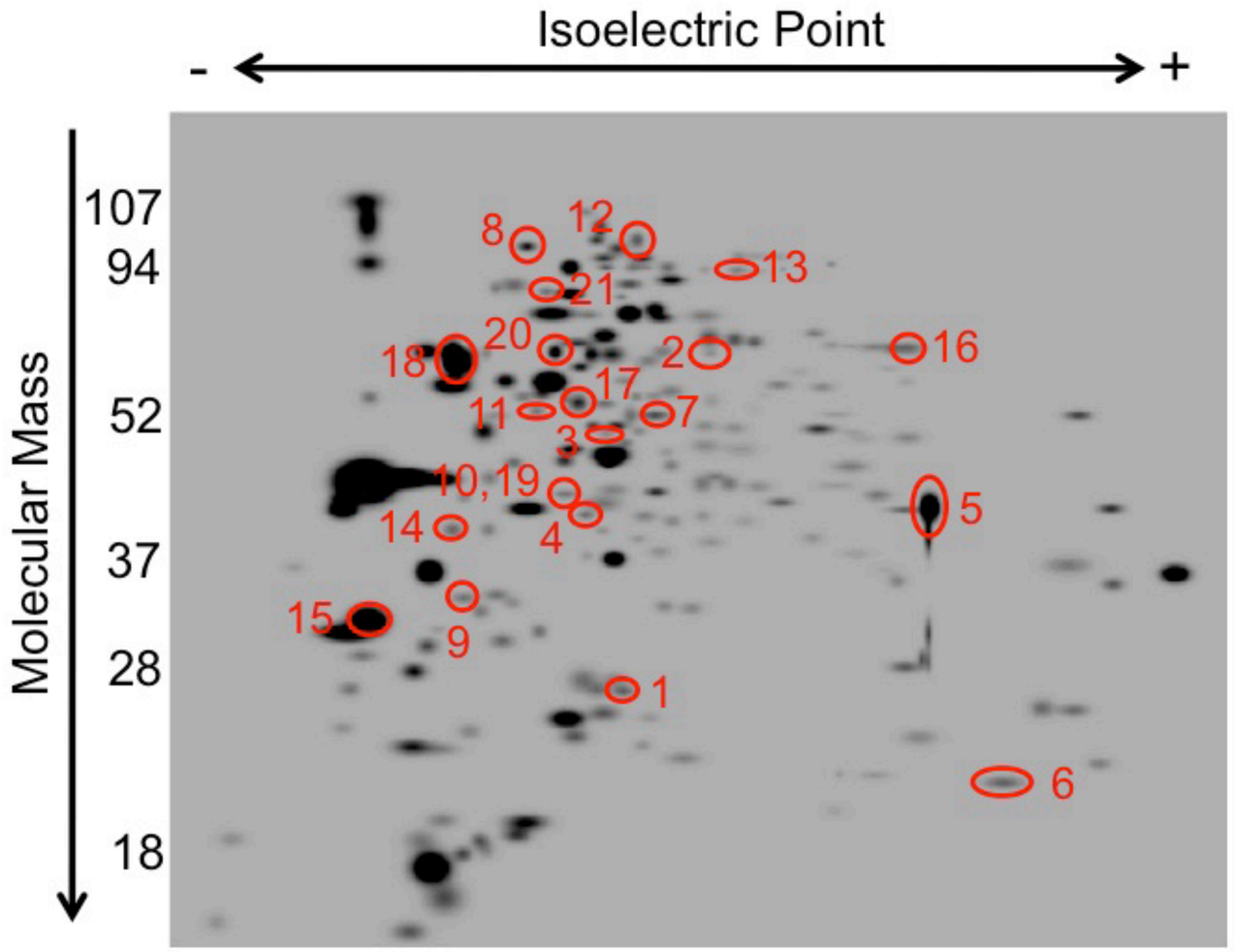
Isoelectric Point
-
+
Molecular Mass
107
94
52
37
28
18
8
12
13
21
20
18
2
16
17
11
7
3
10, 19
5
14
4
15
9
1
6

Figure 2

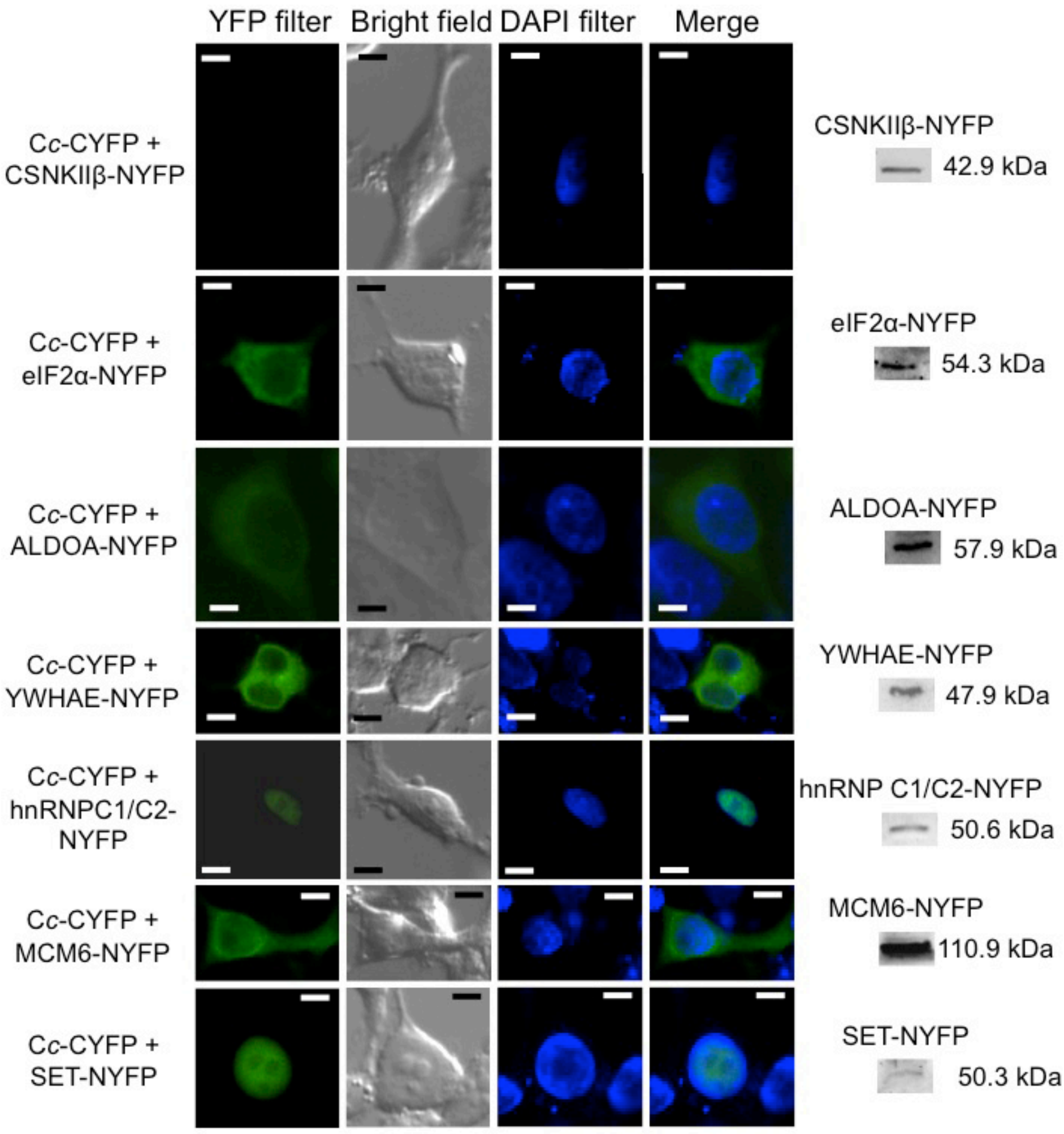
YFP filter
Bright field
DAPI filter
Merge
Cc-CYFP + CSNKIIβ-NYFP
CSNKIIβ-NYFP
42.9 kDa
Cc-CYFP + eIF2α-NYFP
eIF2α-NYFP
54.3 kDa
Cc-CYFP + ALDOA-NYFP
ALDOA-NYFP
57.9 kDa
Cc-CYFP + YWHAE-NYFP
YWHAE-NYFP
47.9 kDa
Cc-CYFP + hnRNPC1/C2-NYFP
hnRNP C1/C2-NYFP
50.6 kDa
Cc-CYFP + MCM6-NYFP
MCM6-NYFP
110.9 kDa
Cc-CYFP + SET-NYFP
SET-NYFP
50.3 kDa

Figure 2 (cont.)

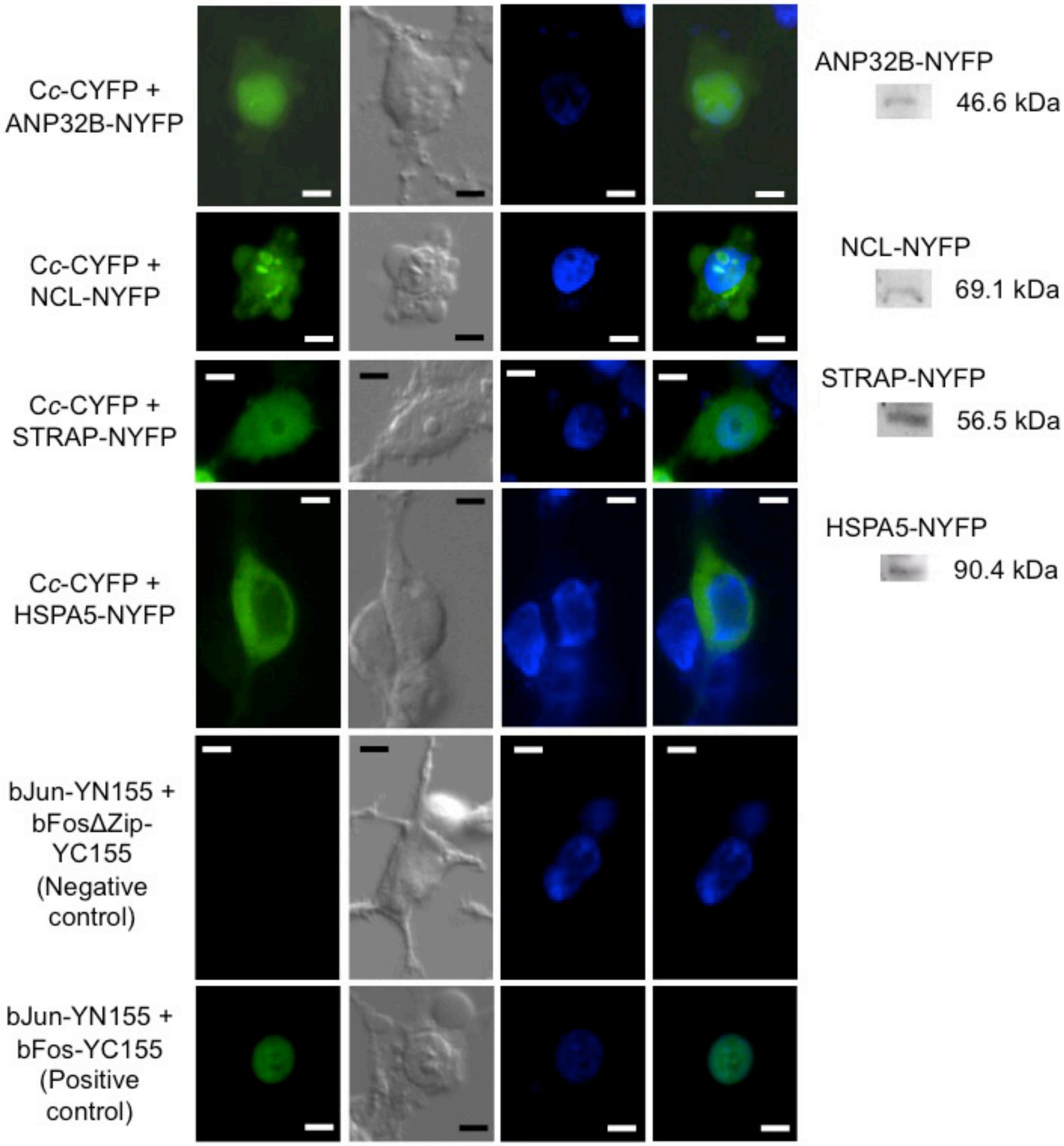

A

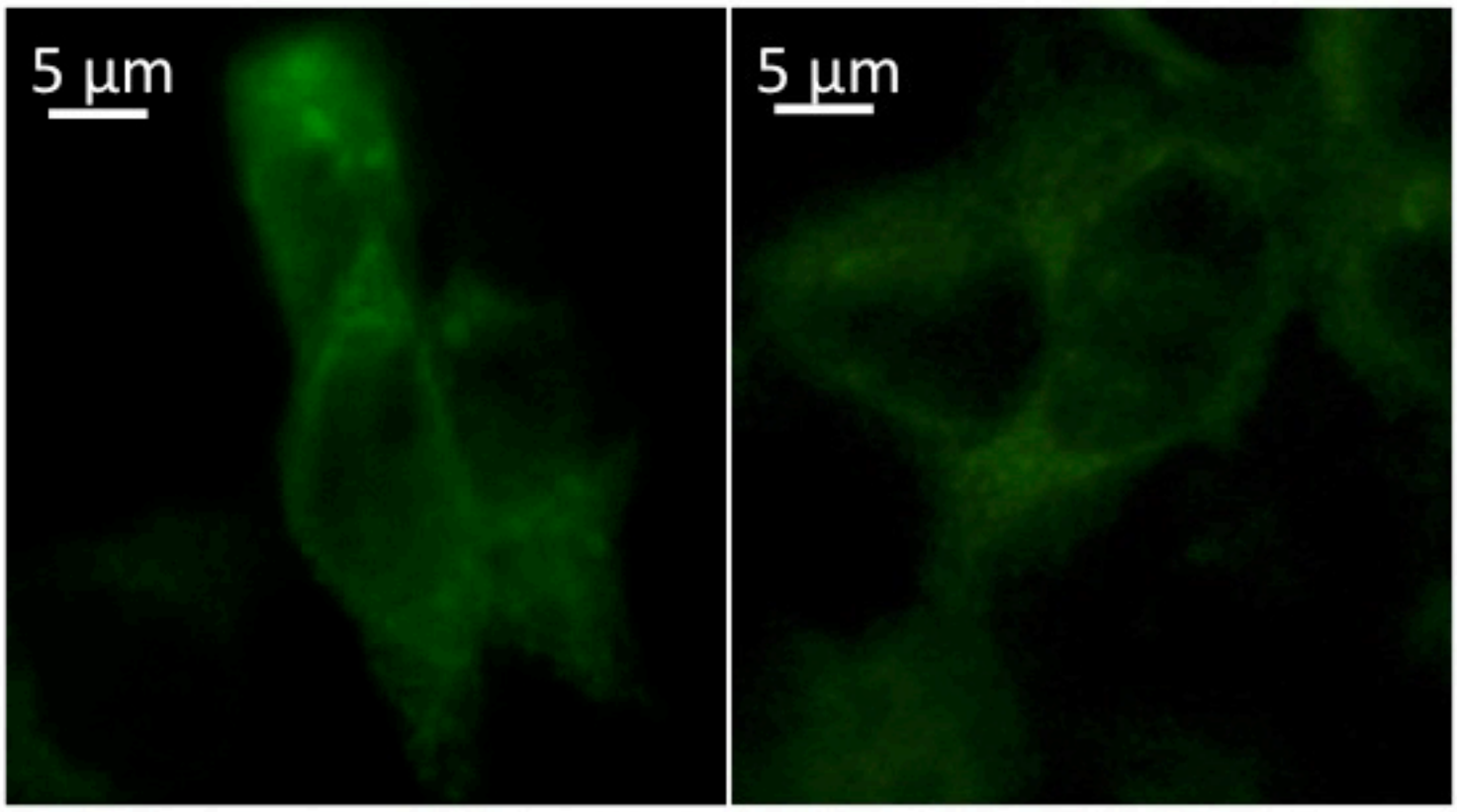

B

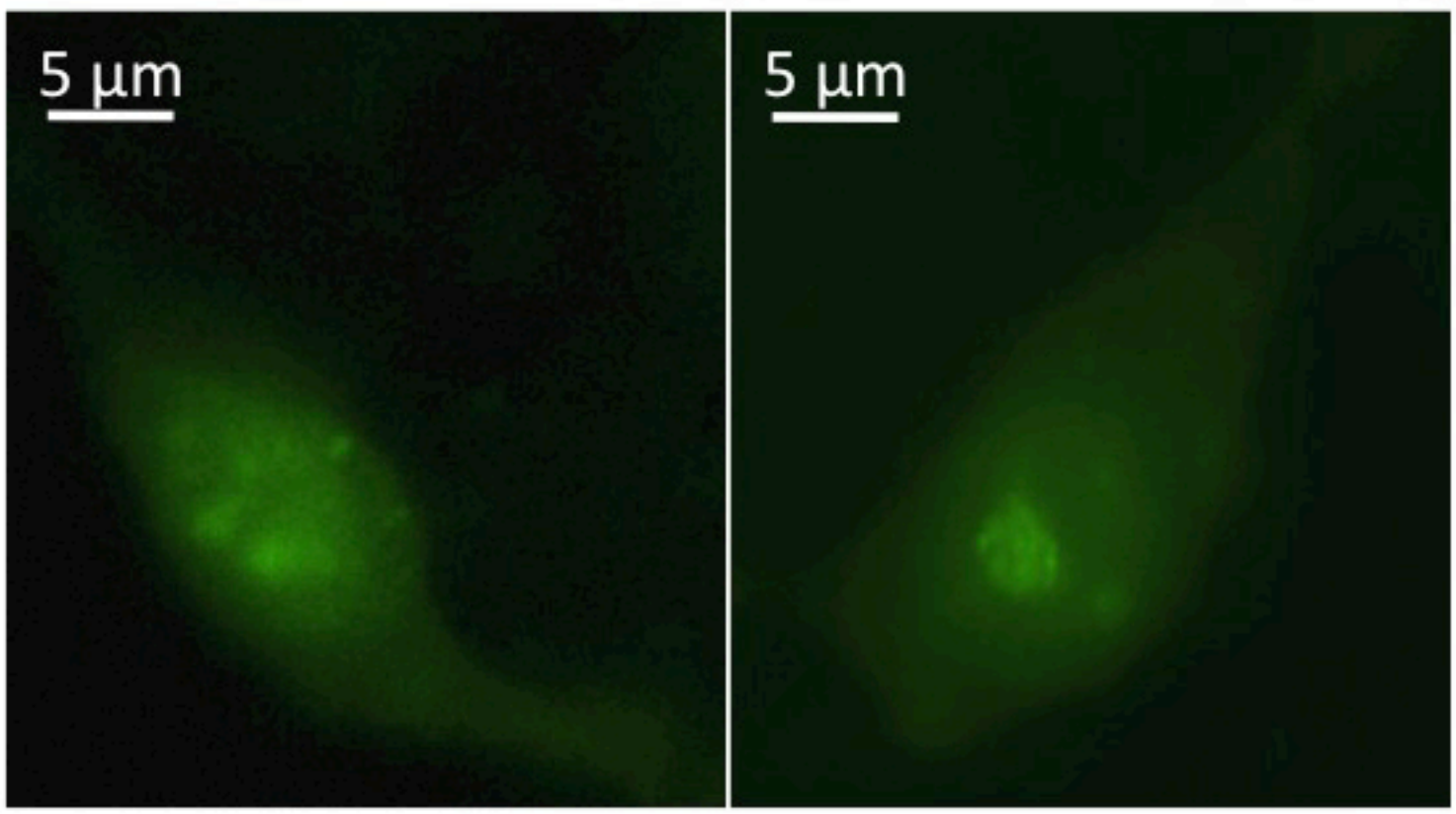

C

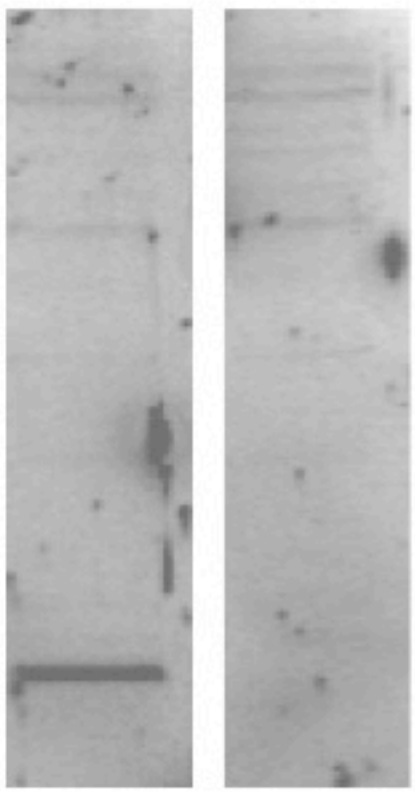

Cc-CYFP

Figure 3

Figure 4

A

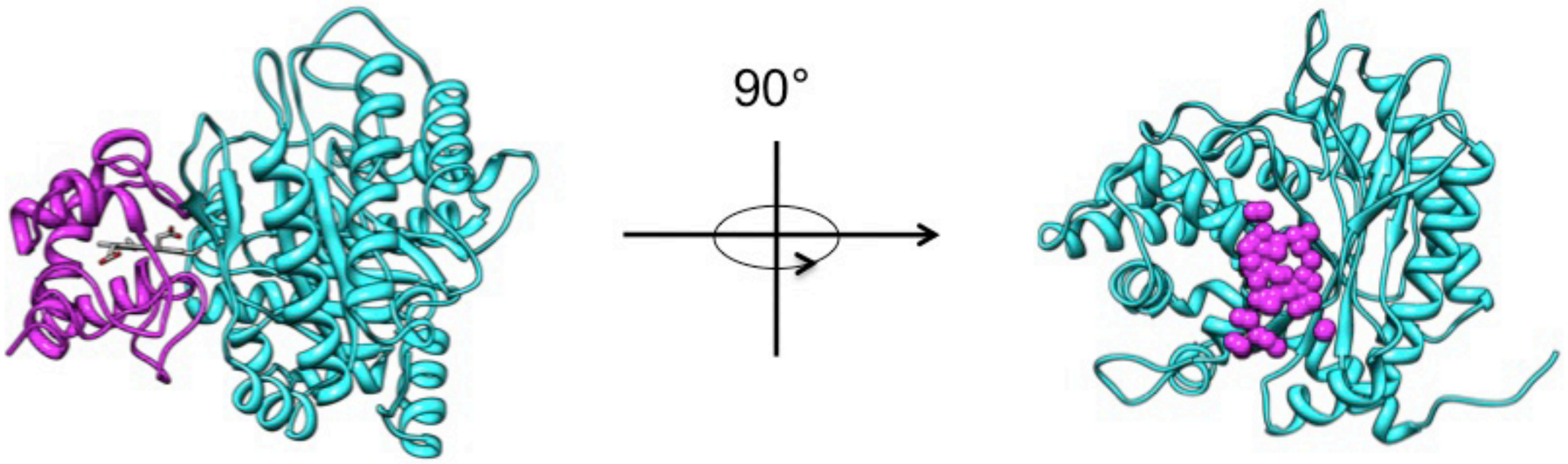

B

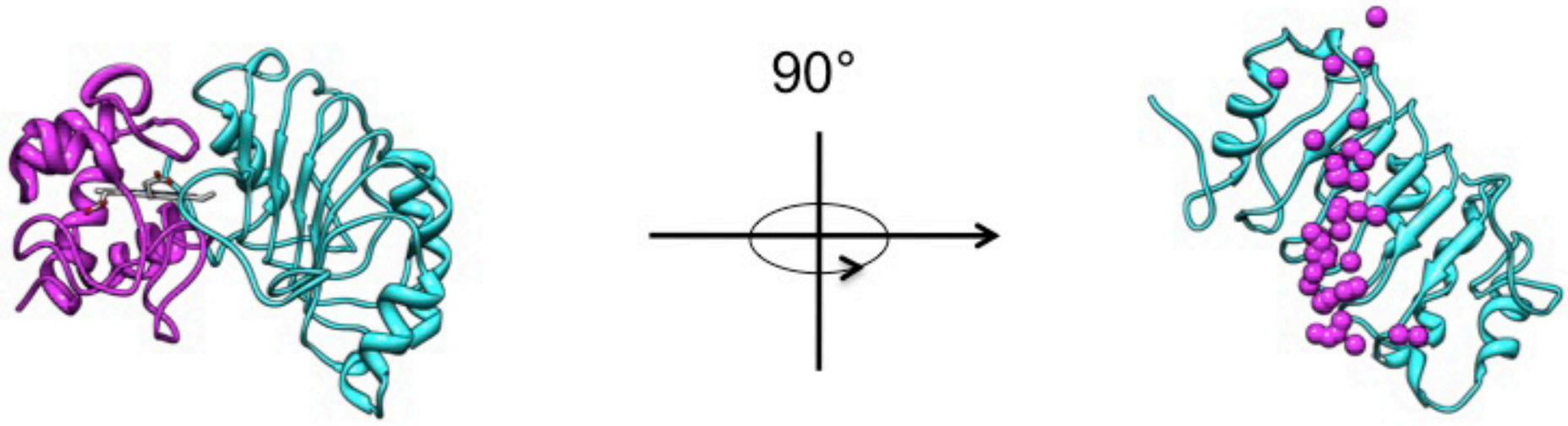

C

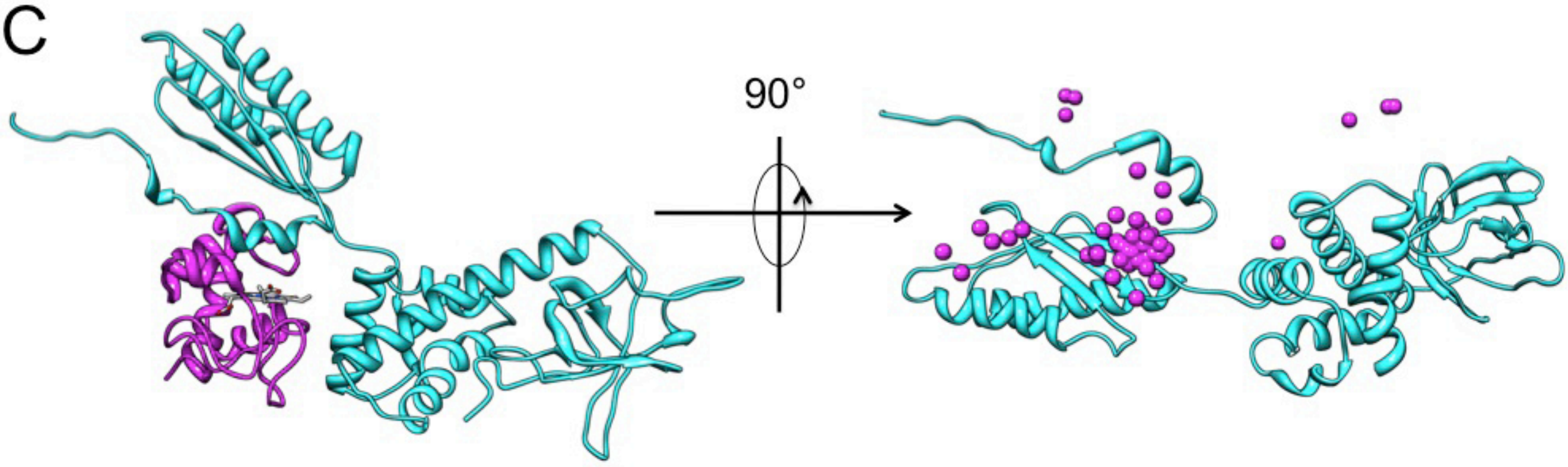

D

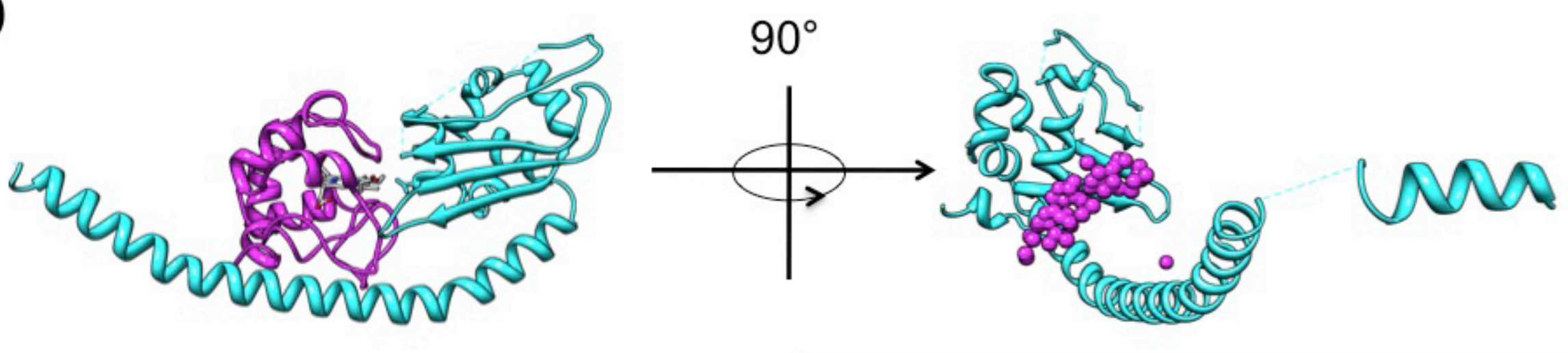

E

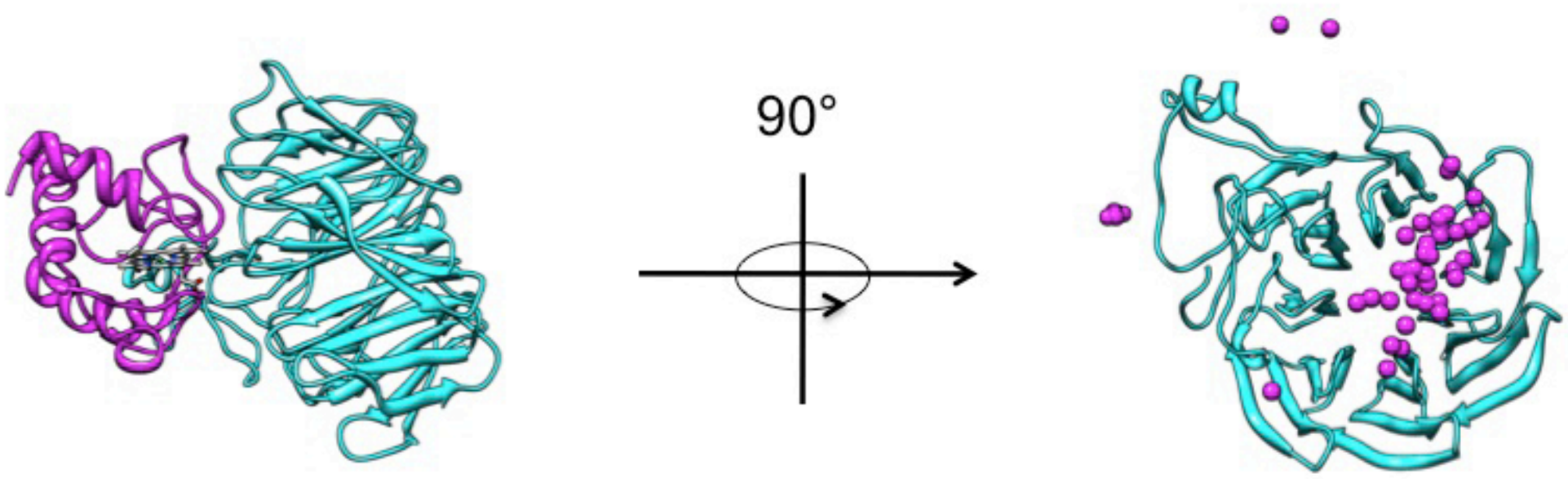

F

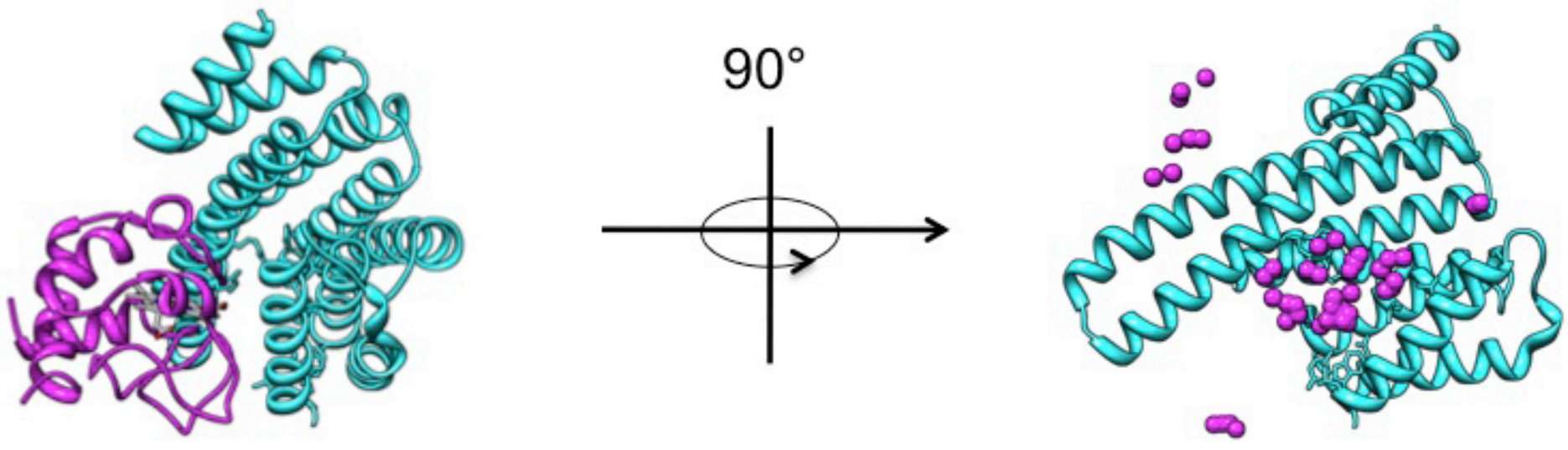

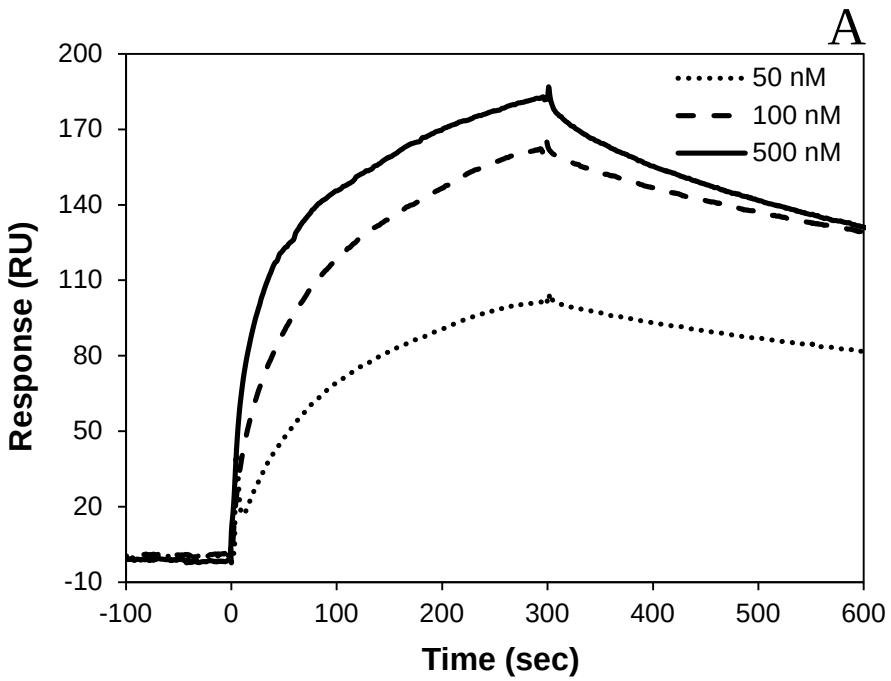
A
50 nM
100 nM
500 nM
Response (RU)
Time (sec)
200
170
140
110
80
50
20
-10
-100
0
100
200
300
400
500
600

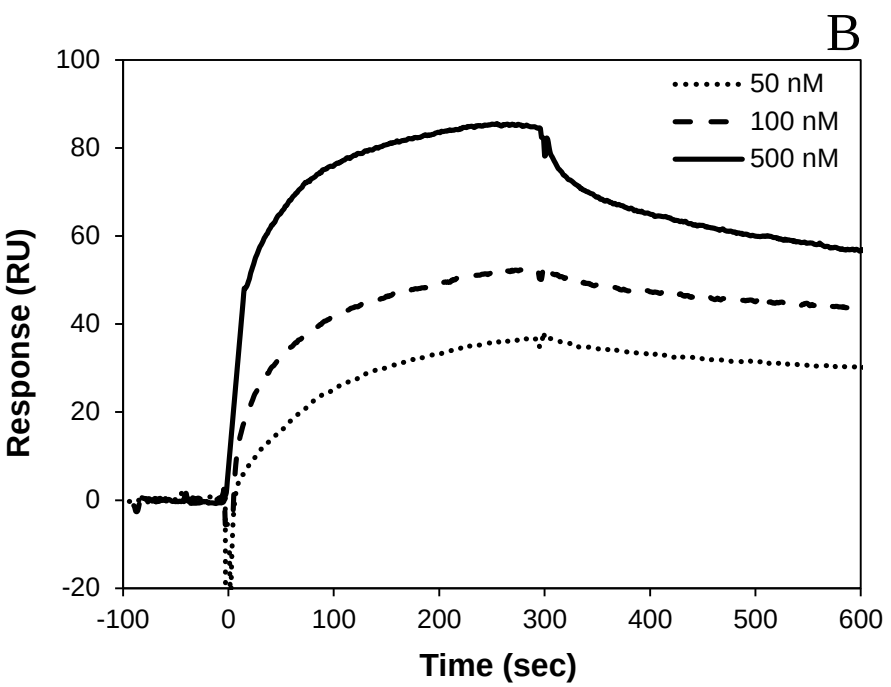
B
50 nM
100 nM
500 nM
Response (RU)
Time (sec)
100
80
60
40
20
0
-20
-100
0
100
200
300
400
500
600

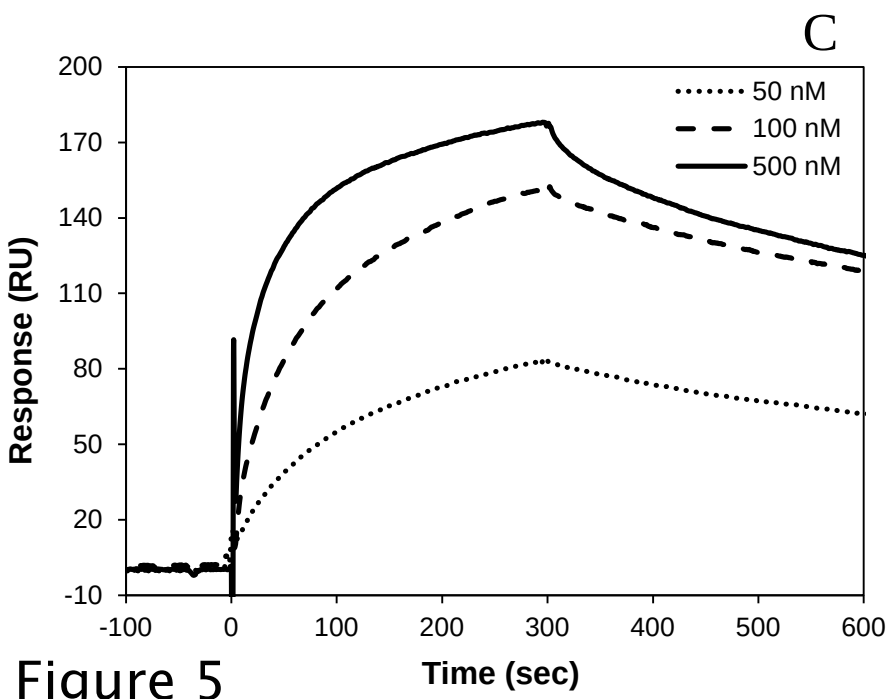
C
50 nM
100 nM
500 nM
Response (RU)
Time (sec)
200
170
140
110
80
50
20
-10
-100
0
100
200
300
400
500
600

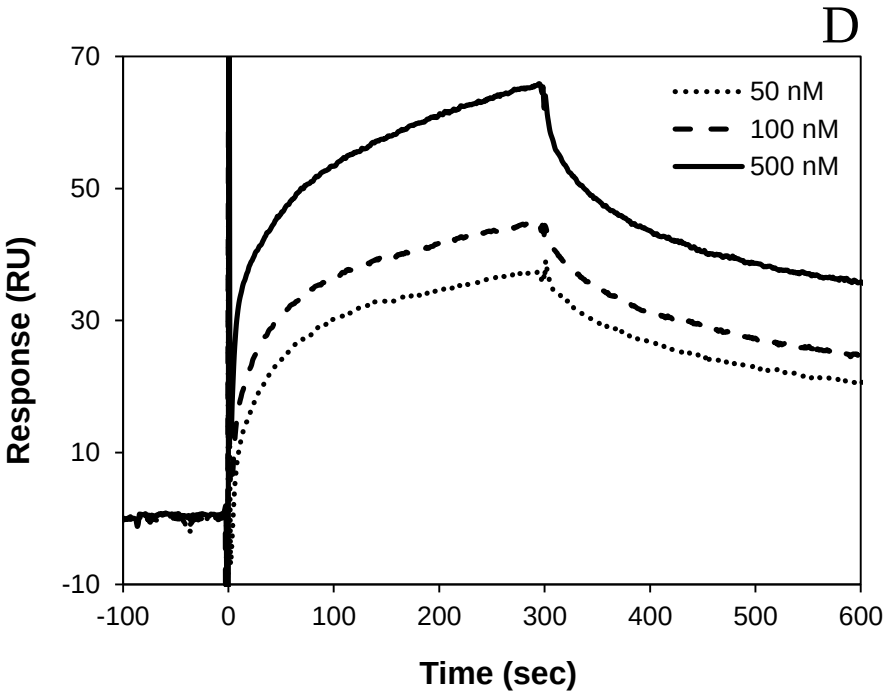
D
50 nM
100 nM
500 nM
Response (RU)
Time (sec)
70
50
30
10
-10
-100
0
100
200
300
400
500
600

Figure 5

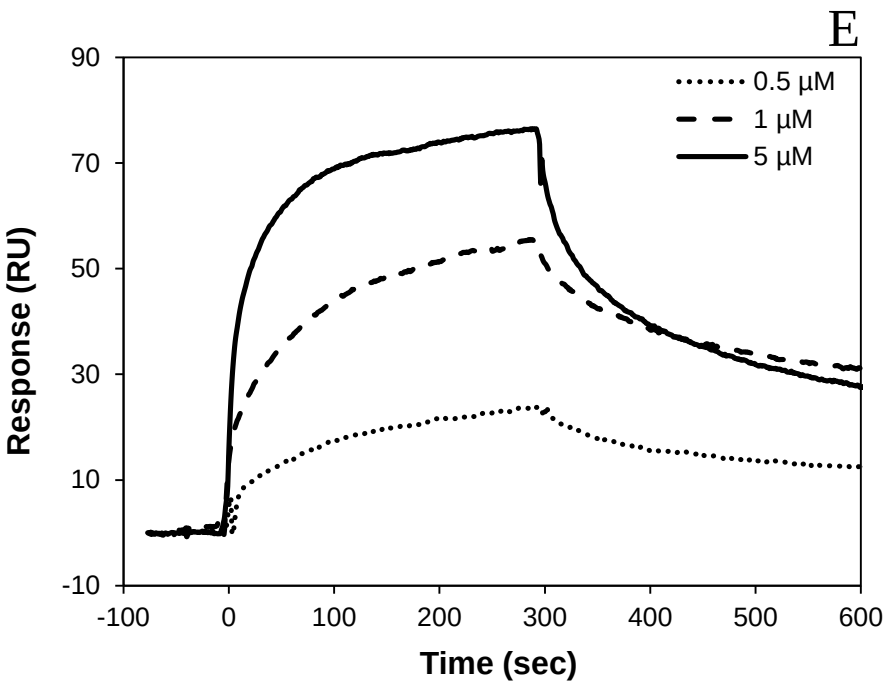

Figure 5. Cont.

Figure 6

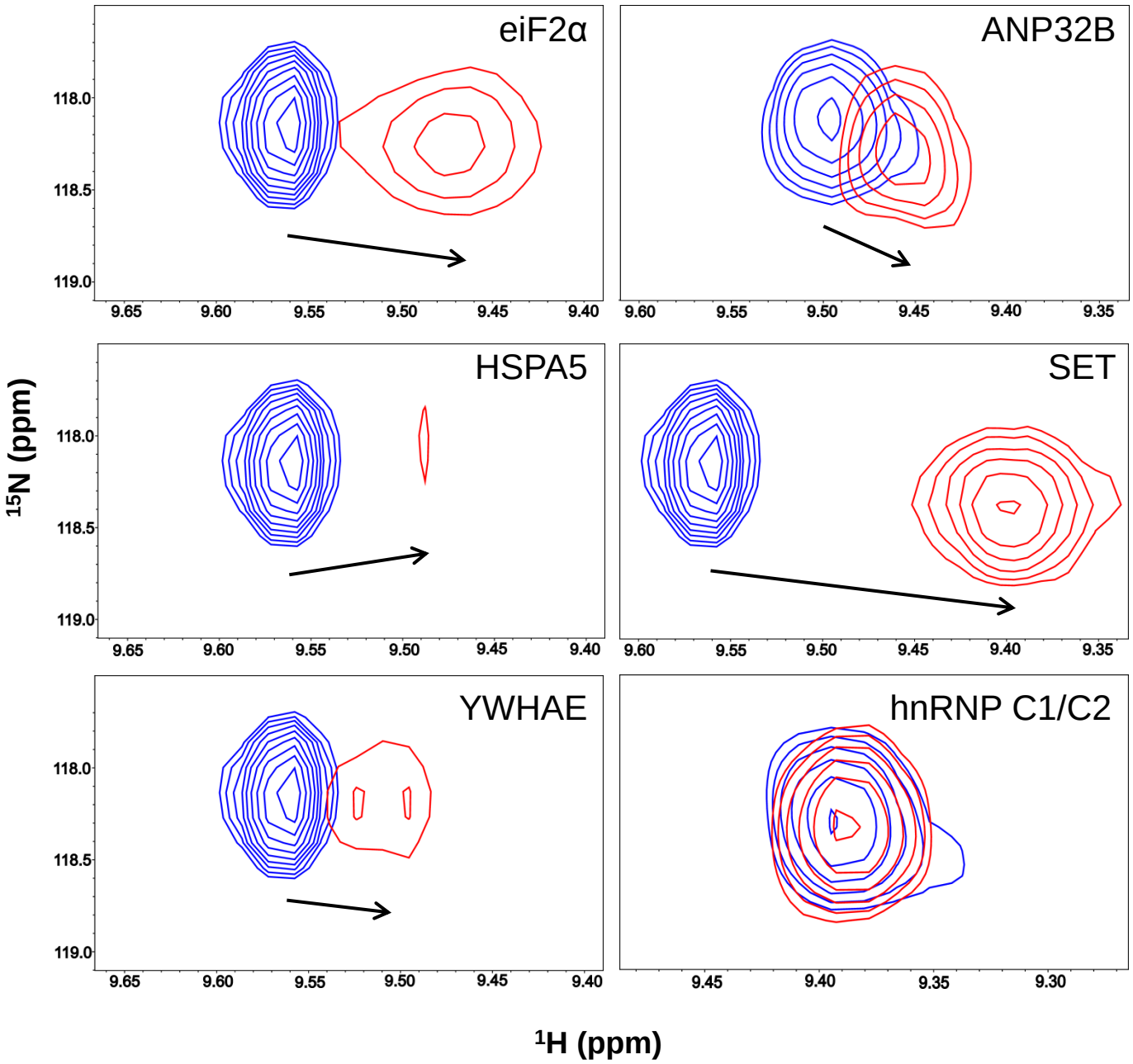
eiF2α
ANP32B
HSPA5
SET
YWHAE
hnRNP C1/C2
118.0
118.5
119.0
9.65
9.60
9.55
9.50
9.45
9.40
9.35
9.30
15N (ppm)
1H (ppm)

Figure 7

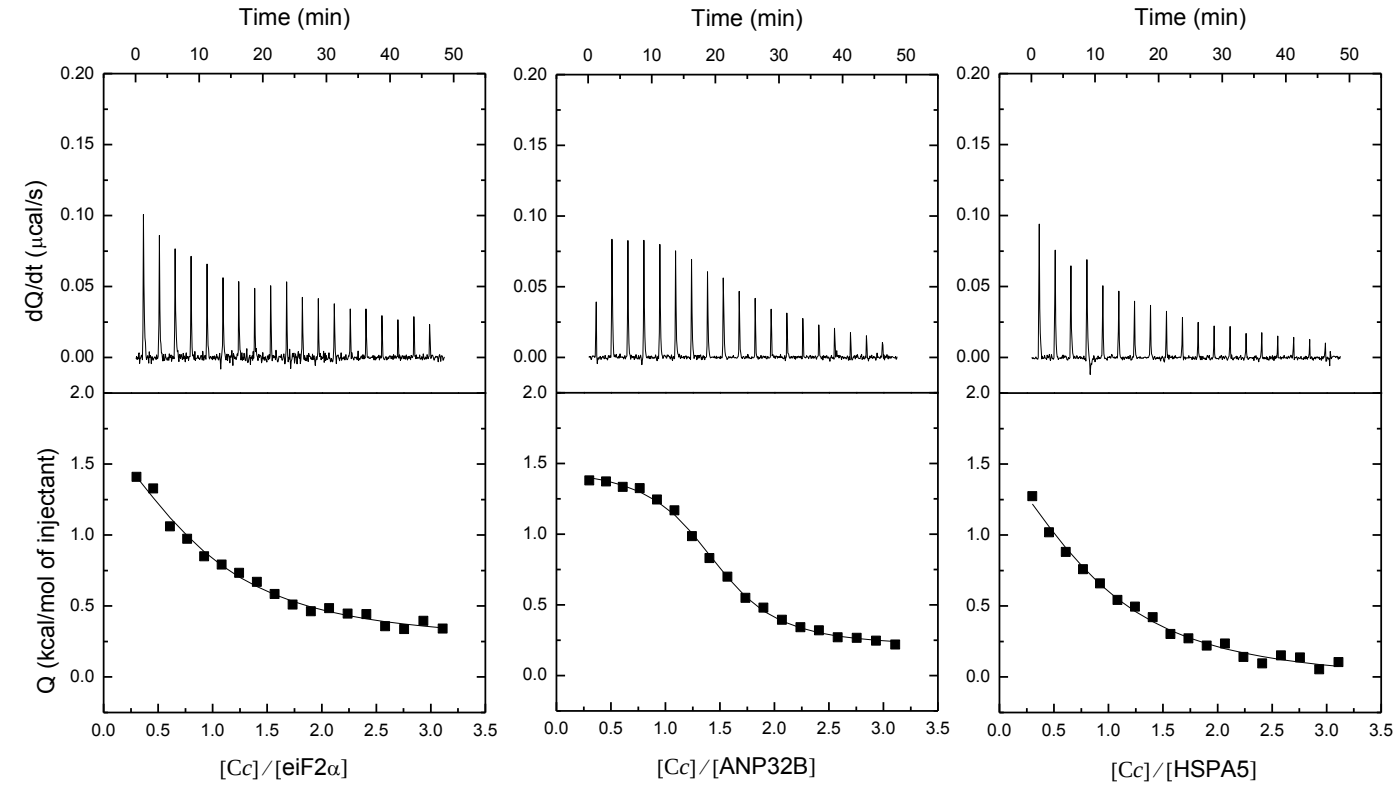
Time (min)
dQ/dt (μcal/s)
Q (kcal/mol of injectant)
[Cc]/[eiF2α]
[Cc]/[ANP32B]
[Cc]/[HSPA5]

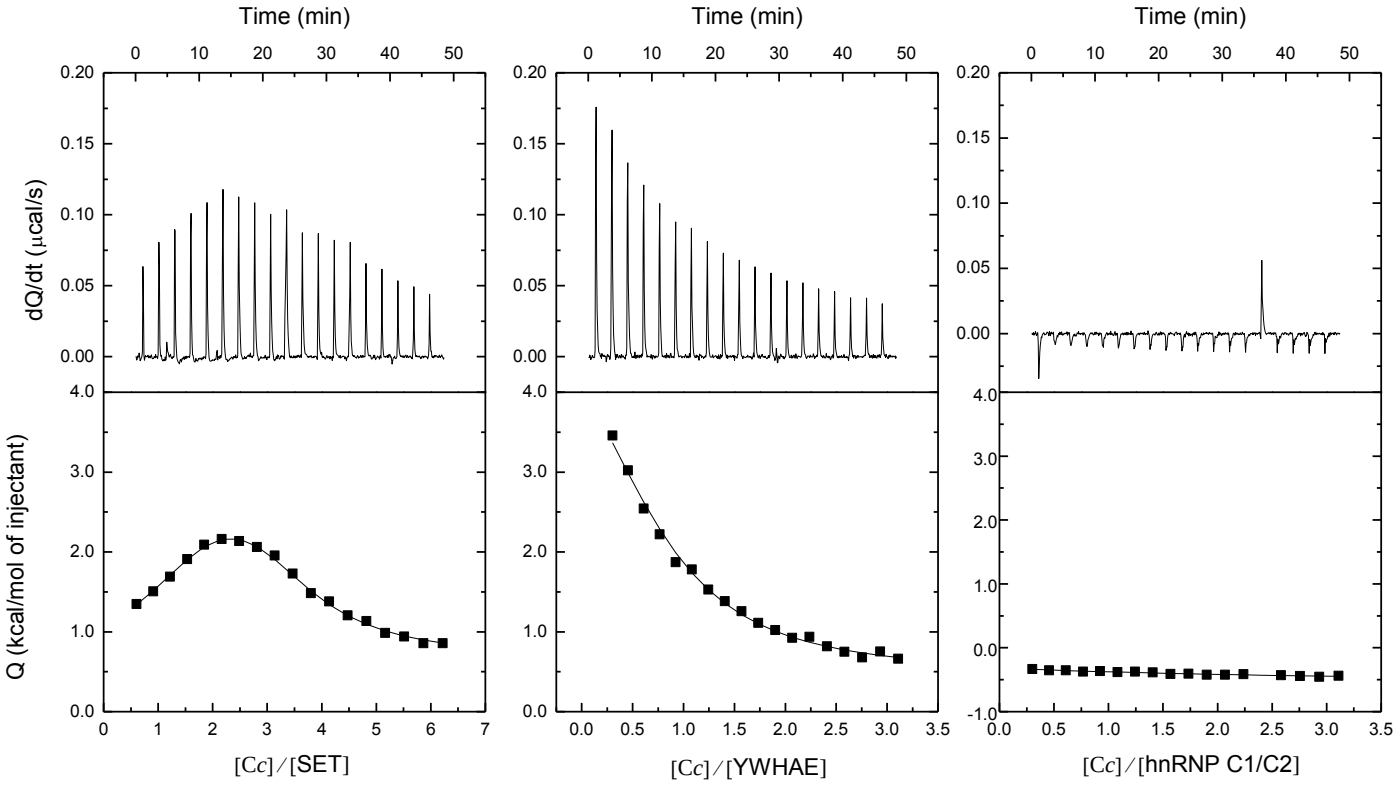
Time (min)
dQ/dt (μcal/s)
Q (kcal/mol of injectant)
[Cc]/[SET]
[Cc]/[YWHAE]
[Cc]/[hnRNP C1/C2]

Figure 8

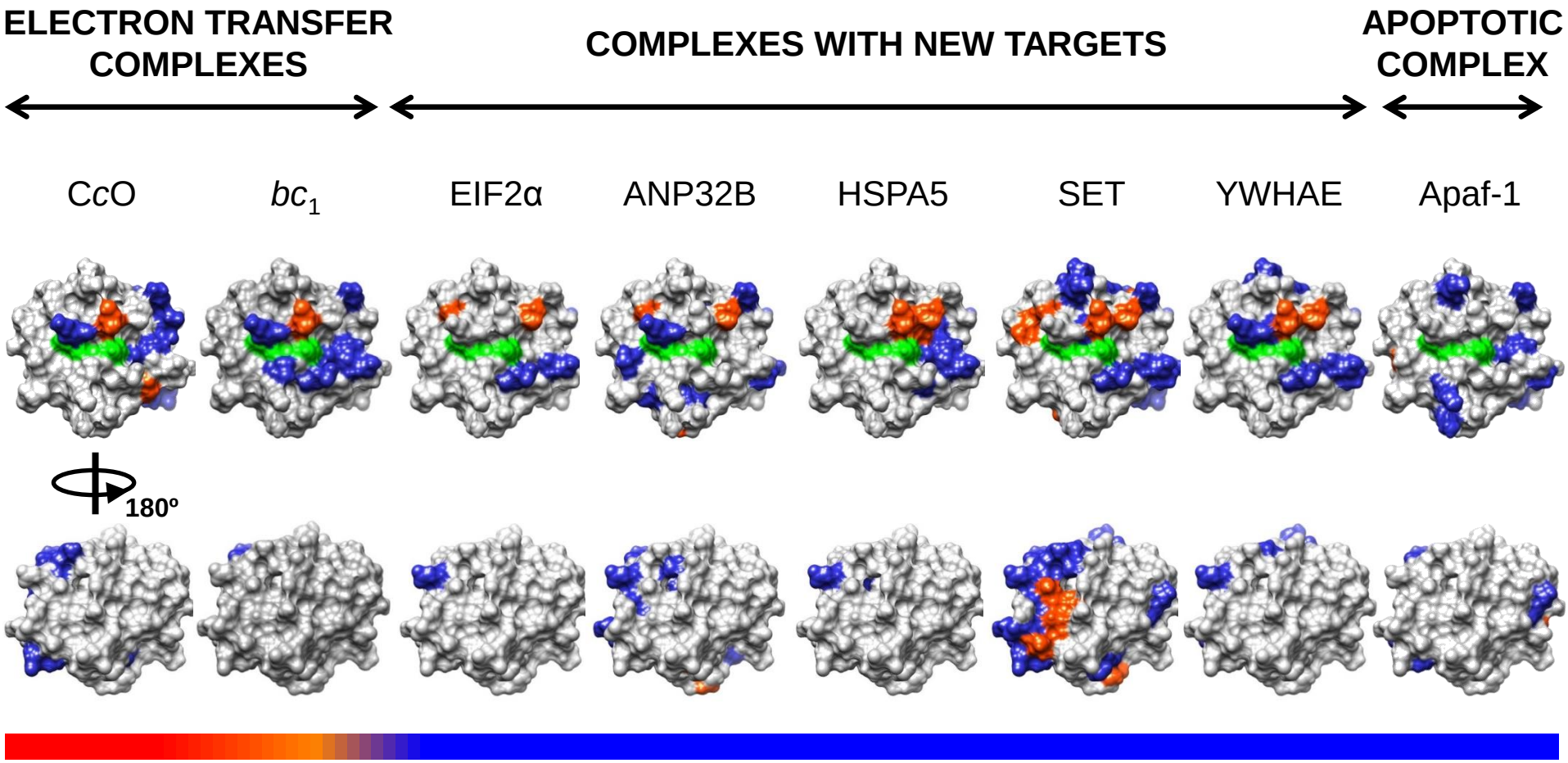
ELECTRON TRANSFER COMPLEXES
COMPLEXES WITH NEW TARGETS
APOPTOTIC COMPLEX
CcO
bc1
EIF2α
ANP32B
HSPA5
SET
YWHAE
Apaf-1
180º

Figure 9

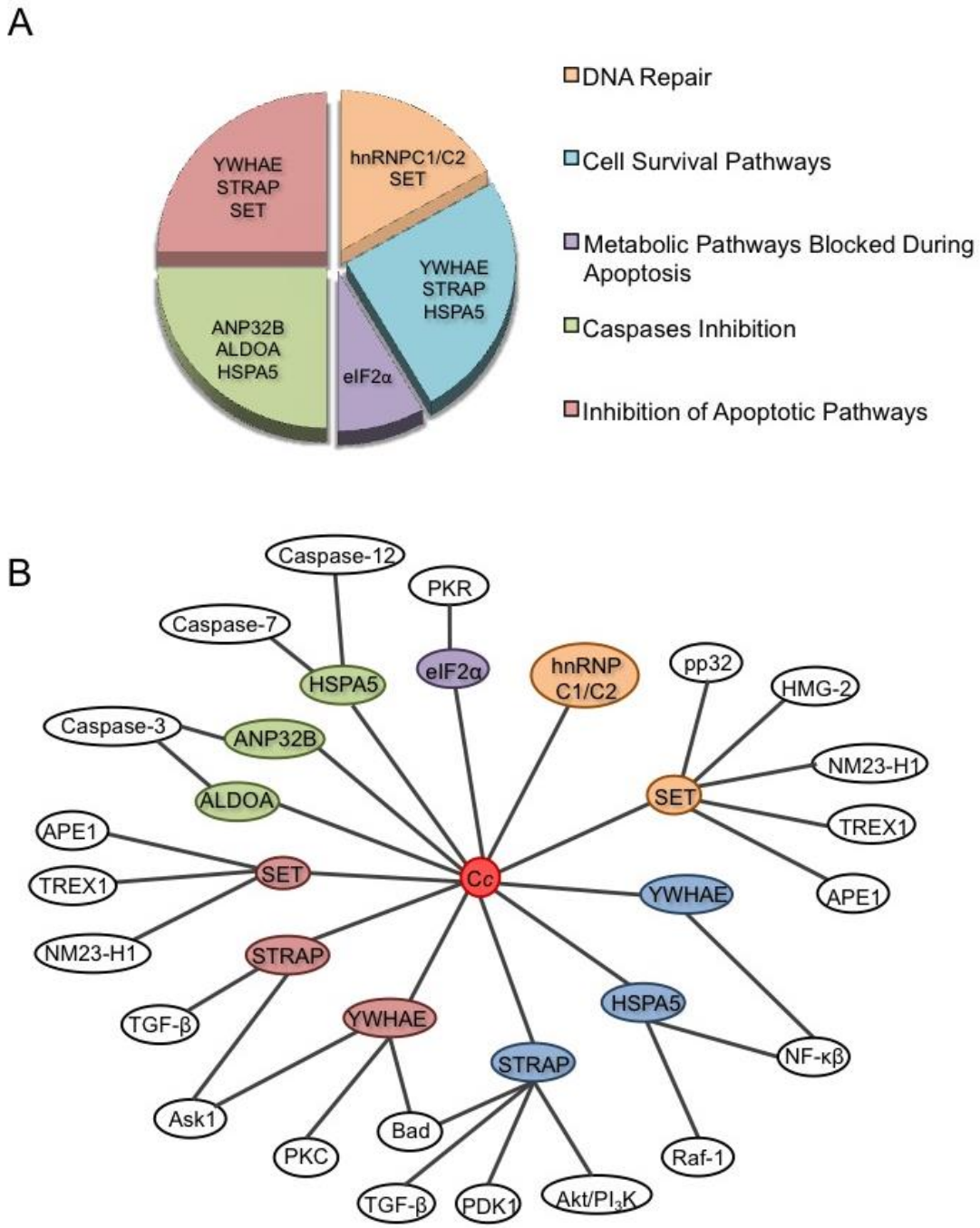
A
YWHAE
STRAP
SET
hnRNPC1/C2
SET
YWHAE
STRAP
HSPA5
ANP32B
ALDOA
HSPA5
eIF2α
DNA Repair
Cell Survival Pathways
Metabolic Pathways Blocked During Apoptosis
Caspases Inhibition
Inhibition of Apoptotic Pathways
B
Caspase-12
PKR
Caspase-7
HSPA5
eIF2α
hnRNP C1/C2
pp32
HMG-2
Caspase-3
ANP32B
NM23-H1
ALDOA
SET
APE1
TREX1
TREX1
SET
Cc
YWHAE
APE1
NM23-H1
STRAP
TGF-β
YWHAE
HSPA5
NF-κβ
STRAP
Ask1
Bad
PKC
Raf-1
TGF-β
PDK1
Akt/PI3K